HHS Public Access

Author manuscript

Dev Biol. Author manuscript; available in PMC 2019 December 01.

Published in final edited form as:

Dev Biol. 2018 December 01; 444(Suppl 1): S219–S236. doi:10.1016/j.ydbio.2018.05.002.

FGF and TGFβ signaling link form and function during jaw development and evolution

Katherine C. Woronowicz, **Stephanie E. Gline**, **Safa T. Herfat**, **Aaron J. Fields**, **Richard A. Schneider***

Department of Orthopaedic Surgery, University of California, San Francisco, 513 Parnassus Avenue, S-1161, San Francisco, CA 94143-0514, USA

Abstract

How does form arise during development and change during evolution? How does form relate to function, and what enables embryonic structures to presage their later use in adults? To address these questions, we leverage the distinct functional morphology of the jaw in duck, chick, and quail. In connection with their specialized mode of feeding, duck develop a secondary cartilage at the tendon insertion of their jaw adductor muscle on the mandible. An equivalent cartilage is absent in chick and quail. We hypothesize that species-specific jaw architecture and mechanical forces promote secondary cartilage in duck through the differential regulation of FGF and TGFβ signaling. First, we perform transplants between chick and duck embryos and demonstrate that the ability of neural crest mesenchyme (NCM) to direct the species-specific insertion of muscle and the formation of secondary cartilage depends upon the amount and spatial distribution of NCM-derived connective tissues. Second, we quantify motility and build finite element models of the jaw complex in duck and quail, which reveals a link between species-specific jaw architecture and the predicted mechanical force environment. Third, we investigate the extent to which mechanical load mediates FGF and TGFβ signaling in the duck jaw adductor insertion, and discover that both pathways are mechanoresponsive and required for secondary cartilage formation. Additionally, we find that FGF and TGFβ signaling can also induce secondary cartilage in the absence of mechanical force or in the adductor insertion of quail embryos. Thus, our results provide novel insights on molecular, cellular, and biomechanical mechanisms that couple musculoskeletal form and function during development and evolution.

Keywords

Avian jaw development and evolution; Form and function; Chimeras; Neural crest; Secondary cartilage; Coronoid process; Mechanical environment; Finite element analysis

*Corresponding author. rich.schneider@ucsf.edu (R.A. Schneider).

Author contributions

R.A.S. and K.C.W. conceived of the project and designed the experiments; K.C.W. S.G., and S.H. performed the experiments; K.C.W. S.G., S.H., A.F., and R.A.S. analyzed the data; and R.A.S. and K.C.W. co-wrote the manuscript.

1. Introduction

One of the most remarkable aspects of being an embryo, and a phenomenon that has intrigued embryologists since Aristotle, is the ability to grow in a manner “rather prospective than retrospective” (Thompson, 1942). In theory, how the form of an embryo can presage later adult function is explained by Aristotle’s observation that “the organism is the τελος, or final cause, of its own process of generation and development” (Thompson, 1942). But elucidating precise molecular mechanisms that link form and function, and specifically resolving whether form arises from function or function follows form remains challenging, because, like the chicken and the egg, form and function are seamlessly intertwined during development and evolution.

Some of the most illustrious instances of form and function appear in the craniofacial complex of birds, which are masters of adaptation. A specialized beak seems to exist for every avian diet: insectivore, granivore, nectarivore, frugivore, carnivore, omnivore, etc. (Schneider, 2007; Zusi, 1993). Each diet is supported by a range of structural adaptations to the jaw including size, shape, and sites of muscle attachments (Fish and Schneider, 2014b; Tokita and Schneider, 2009). For example, in *Anseriformes*, or waterfowl such as duck, which use their broad bills to dredge sediment for food, the mandibular adductor muscle attaches laterally to a large protruding coronoid process on the mandible. Such a configuration provides a robust insertion site for transmitting the high magnitude forces associated with suction pump and levered straining jaw movements (Dawson et al., 2011; Zweers, 1974; Zweers et al., 1977b). In duck, as in humans, the coronoid process develops via a secondary cartilage intermediate (Solem et al., 2011). Secondary cartilage requires proper mechanical stimulation for its induction and maintenance, as confirmed by explant cultures and paralysis experiments, and is a feature of many joints in neognathic avian skulls, as well as in select tendon and muscle insertions (Hall, 1967, 1968, 1972, 1986). In paralyzed duck, secondary cartilage fails to form at the coronoid process, suggesting that the mechanical environment (i.e., function) during development promotes secondary chondrogenesis (Solem et al., 2011). By comparison, *Galliformes* like quail and chick, feed primarily by pecking seed, and this is reflected in the relatively gracile construction of the jaw and adductor muscles, which insert dorsally on the mandible and lack secondary cartilage on the coronoid process (Baumel, 1993; Chamberlain, 1943; Fitzgerald, 1969; Jollie, 1957; Lucas and Stettenheim, 1972; McLeod, 1964; Shufeldt, 1909; Van den Heuvel, 1992). Exploiting such species-specific differences in quail and duck, as we have done previously in studies of beak, feather, cartilage, bone, and muscle patterning (Ealba et al., 2015; Eames and Schneider, 2008; Fish and Schneider, 2014a; Hall et al., 2014; Schneider, 2005, 2015; Schneider and Helms, 2003; Tokita and Schneider, 2009), provides an opportunity to investigate molecular, cellular, and biomechanical mechanisms that integrate form and function in the jaw apparatus during development and evolution.

The species-specific jaw morphology that distinguishes duck from quail is mediated by the neural crest mesenchyme (NCM), which gives rise to all of the associated cartilage, bone, and muscle connective tissues (Noden and Schneider, 2006). Transplanting presumptive NCM from quail into duck has established that NCM controls the size and shape of the jaw skeleton, as well as the orientation and insertion of muscles (Ealba et al., 2015; Eames

and Schneider, 2008; Fish and Schneider, 2014a; Hall et al., 2014; Schneider and Helms, 2003; Solem et al., 2011; Schneider, 2018a, 2018b; Tokita and Schneider, 2009). Chimeric "quck" develop a quail-like jaw musculoskeleton including a dorsal mandibular adductor insertion that lacks secondary cartilage. The precise developmental mechanisms through which this happens have remained an open question. Presumably, for such a transformation, quail NCM alters the duck-host environment in a manner that changes not only the form of the jaw apparatus but also the function, since the presence or absence of secondary cartilage depends upon proper mechanical cues. In this context, the lateral versus dorsal insertion of the mandibular adductor muscle might produce distinct mechanical forces, but differences in the quantity and/or quality of such forces in quail versus duck are completely unknown. Furthermore, those signaling pathways that are mechanoresponsive and ultimately govern species-specific adaptation to the mechanical environment remain unclear. The current study set out to address these unresolved issues.

We hypothesized that the form of the duck mandibular adductor complex creates a species-specific mechanical environment, which activates molecular programs for secondary chondrogenesis at the coronoid process. To test our hypothesis, we employed a range of strategies. We modulated the form of the duck mandibular adductor complex by titrating the amount of donor versus host NCM-derived tissues in chick-duck chimeras. We quantified embryonic jaw motility in duck versus quail and performed finite element analysis (FEA) to model the mechanical environment of the mandibular adductor complex. We employed FEA in order to make predictions about the extent to which mechanical forces might underlie the induction of secondary cartilage and the differential regulation of mechanically responsive signaling pathways. We disrupted the mechanical environment of the mandibular adductor complex by paralyzing duck embryos and then we assayed for changes in signaling pathways that might be mechanically responsive at the coronoid process. After identifying candidate pathways, we tested if they were necessary and/or sufficient for the formation of secondary cartilage.

Our results reveal that the formation of secondary cartilage on the coronoid process depends upon the amount and spatial distribution of NCM-derived connective tissues. While we observe few quantitative differences in the amount of motility between quail and duck, our FEA suggests that quail and duck have qualitatively distinct mechanical forces at the mandibular adductor insertion. Given the potential for species-specific variation in the mechanical force environment of quail versus duck, we assayed for the differential regulation and involvement of the Fibroblast Growth Factor (FGF) and Transforming Growth Factor-Beta (TGFβ) pathways in the induction of secondary cartilage on the duck coronoid process, since these are both known to play a role during mechanotransduction and chondrogenesis in other biological contexts (Balooch et al., 2005; Chang et al., 2010; Derynck et al., 2008; Govindarajan and Overbeek, 2006; Lorda-Diez et al., 2009; Murakami et al., 2000; Robbins et al., 1997a). We find that both FGF and TGFβ signaling are responsive to mechanical forces within the duck mandibular adductor complex, and are necessary for secondary chondrogenesis at the coronoid process. Additionally, we find that exogenous FGF and TGFβ ligands can rescue cartilage in paralyzed duck and also induce cartilage in the quail mandibular adductor insertion, where ordinarily there is none. Overall, this study provides mechanistic insights on how species-specific morphology, mechanical

forces, and resultant changes in signaling activity become integrated and contribute to musculoskeletal plasticity. While form initially dictates function, function can also act as a potent modulator of musculoskeletal form during development and evolution.

2. Methods

2.1. The use of avian embryos

Fertilized eggs of Japanese quail (*Coturnix coturnix japonica*) and white Pekin duck (*Anas platyrhynchos*) were purchased from AA Lab Eggs (Westminster, CA) and incubated at 37.5 °C in a humidified chamber (GQF Hova-Bator, Savannah, GA) until embryos reached stages appropriate for manipulations, treatments, and analyses. For all procedures, we adhered to accepted practices for the humane treatment of avian embryos as described in S3.4.4 of the AVMA Guidelines for the Euthanasia of Animals: 2013 Edition (Leary et al., 2013). Embryos were stage-matched using an approach that is based on external morphological characters and that is independent of body size and incubation time (Hamilton, 1965; Ricklefs and Starck, 1998; Starck and Ricklefs, 1998). The Hamburger and Hamilton (HH) staging system, originally devised for chick, is a well-established standard (Hamburger and Hamilton, 1951). Separate staging systems do exist for duck (Koecke, 1958) and quail (Ainsworth et al., 2010; Nakane and Tsudzuki, 1999; Padgett and Ivey, 1960; Zacchei, 1961) but these embryos can also be staged via the HH scheme used for chicken (Ainsworth et al., 2010; Le Douarin et al., 1996; Lwigale and Schneider, 2008; Mitgutsch et al., 2011; Schneider and Helms, 2003; Smith et al., 2015; Starck, 1989; Yamashita and Sohal, 1987; Young et al., 2014). Criteria utilized to align quail and duck at a particular HH stage change over time depending on which structures become prominent. For early embryonic stages, we used the extent of neurulation, NCM migration, and somitogenesis as markers (Fish et al., 2014; Lwigale and Schneider, 2008; Schneider and Helms, 2003); whereas later, we relied on growth of the limbs, facial primordia, feather buds, and eyes since these become more diagnostic (Eames and Schneider, 2005; Merrill et al., 2008).

2.2. Histology

Embryos were fixed overnight in 10% neutral buffered formalin at 4 °C, paraffin embedded, and sectioned at 10 μm. Cartilage, bone, muscle, and tendon were visualized using Milligan's Trichrome or Safranin-O (Ferguson et al., 1998; Presnell and Schreibman, 1997).

2.3. Clearing and staining

Embryos were fixed overnight at 4 °C in 10% neutral buffered formalin before clearing and staining with Alcian Blue and Alizarin Red to visualize cartilage and bone of the jaw complex including the coronoid process (Wassersug, 1976).

2.4. cDNA preparation

RNA was isolated from microdissected duck samples using the ARCTURUS PicoPure RNA Isolation Kit (ThermoFisher, Waltham, MA). Reaction specifications and reverse transcription programs were followed as previously published (Ealba and Schneider, 2013).

2.5. In situ hybridization

Spatial and temporal patters of gene expression were analyzed by in situ hybridization as previously described (Albrecht et al., 1997; Schneider et al., 2001). Species-specific probes against duck FGF and TGFβ ligands (*Fgf4, Fgf8* (MH359130), *Tgfβ2* (MH359136), *Tgfβ3* (MH359137)), receptors (*Fgfr2* (MH359132), *Fgfr3* (MH359133), *Tgfβr2* (MH359138)), and downstream effectors (*Pea3* (MH359134), *Erm* (MH359128), *and Smad3* (MH359135)), were cloned from duck HH33 cDNA libraries isolated from whole heads (Table S1). Probes were designed to recognize all isoforms. High fidelity Pfu DNA polymerase (Strategene, La Jolla, CA) was used to amplify target genes. The protocol was: step 1, 2 min at 94 °C; step 2, 30 s at 94 °C; step 3, 30 s at 37.5 °C; step 4, 2 min at 72 °C; step 5, repeat steps 2–4 39 times; step 6, 5 min at 72 °C; step 7, hold at 4 °C. PCR products were run on a 1% agarose gel. Bands of the appropriate molecular weight were gel extracted using QIAEX II Gel Extraction Kit (Qiagen, Hilden, Germany). PCR products were ligated into pGEM-T Easy Vector System I (Promega, Madison, WI) or CloneJET PCR Cloning Kit (ThermoFisher, Waltham, MA) and used to transform NEB 5α E. coli cells (New England Biolabs, Ipswitch, MA). Clones were sequenced (McLab, South San Francisco, CA) using a T7 promoter primer. Sequencing results were analyzed using Geneious (Biomatters, Auckland, New Zealand). Once probe sequences were confirmed, DIG-labeled RNA probes were synthesized using DIG RNA labeling mix (Roche, Basel, Switzerland). Cloned species-specific duck probes were used to identify gene expression patterns in embedded and sectioned HH33 and HH36 paralyzed and stage matched control duck.

2.6. TUNEL staining

10 μm tissue sections of duck embryos 24 h after treatment with SU5402, SB431542, or DMSO soaked beads were processed using a fluorescent TUNEL staining kit (Roche, Basel, Switzerland). As a positive control, DNase was added to a subset of DMSO-treated tissue sections. The percentage of cell death was quantified using 3D microscopy processing software Imaris (Bitplane, Belfast, United Kingdom). Image intensity was rendered in 3D and Hoescht (Sigma-Aldrich, St. Louis, MO) and TUNEL-stained nuclei within 100 μm of the implanted bead were counted using software-enabled volumetric criteria (surface detail = 5 μm, background subtraction = 12 μm, seed point diameter = 30 μm). Statistical significance was determined by ordinary one-way ANOVA (Prism 7, GraphPad Software, Inc., La Jolla, CA).

2.7. Surgical bead implantation

10 mM of SU5402 (Sigma-Aldrich, St. Louis, MO), a small molecule that prevents autophosphorylation of receptor tyrosine kinases and is most specific to FGFRs (Sun et al., 1999, 1998), and 100 mM of SB431542 (Santa Cruz Biotechnology, Santa Cruz, CA), a small molecule that inhibits autophosphorylation of TGFβRs (Callahan et al., 2002; Inman et al., 2002), were diluted in DMSO. Formate bound AG1-X2 (50–100 mesh, 250–850 μm, Bio-Rad, Hercules, CA) beads of about 250–350 μm were washed in DMSO at room temperature for about ten minutes before binding small molecule inhibitors. 1 mg/ml recombinant human FGF4 (R & D Systems, Minneapolis, MN) was re-suspended

in 0.1% filter sterilized BSA in 1× PBS. Heparin acrylic beads about 250–350 μm (Sigma-Aldrich, St. Louis, MO) were used to deliver FGF4 to duck embryos. A 160 μg/ml solution containing equal parts recombinant human TGFβ2 and TGFβ3 (R & D Systems, Minneapolis, MN) was prepared using filter sterilized 4 mM HCl in PBS containing 0.1% BSA. Affigel Blue beads about 250–300 μm (50–100 mesh, 150–300 μm, BioRad, Hercules, CA) were used to deliver TGFβ ligands to quail and duck embryos. Both FGF4 bound heparin acrylic beads and TGFβ2 and TGFβ3 bound Affigel Blue beads were implanted into duck embryos to deliver a combination of all three ligands. Beads were soaked in small molecule inhibitors or ligands for one hour at room temperature before implantation. All concentrations were based on those used previously (Eames and Schneider, 2008; Hayamizu et al., 1991; Niswander et al., 1993; Schneider et al., 2001). Stage HH32 and HH33 embryos were housed in room temperature incubators for one hour before surgeries to minimize embryonic motility. For each bead type used, control surgeries were conducted using beads to deliver carrier. All surgically implanted embryos were collected at HH38. Cleared and stained cases with extensive cartilage and/or bone defects were excluded from analysis under the assumption that a malformation in the jaw skeleton would adversely affect the native mechanical environment. Two-tailed Fisher's exact test was used to determine statistical significance (Prism 7, GraphPad).

2.8. Endoscopy and jaw motility quantification

In ovo video footage of quail and duck from HH32 to HH38 was recorded while eggs incubated at 37.5 °C. Video recordings were captured using a 1088 HD High Definition Camera (Stryker, Kalamazoo, MI) with a 4 mm, 30° arthroscope (Stryker, Kalamazoo, MI). A universal, dual-quartz, halogen, fiber-optic light source (CUDA Surgical, Jacksonville, FL) was threaded onto the endoscope to provide illumination. The arthroscope was inserted through a small opening in the incubation chamber until it was submerged in albumin. Embryos were acclimated to the light source for 15 min prior to recording. Three 10-min videos were collected from each embryo. The interval of time from the first jaw movement to 5 s after the last jaw movement was defined as an activity period, similar to a published quantification method (Hamburger et al., 1965). Average percent active time was calculated along with 95% confidence intervals. Significance was determined using an unpaired, two-tailed Holm-Sidak test adjusted for multiple comparisons (Prism 7, GraphPad).

2.9. 3D reconstruction and finite element analysis

To characterize species-specific differences in the biomechanical environment of the jaw adductor complex, linear finite element analysis (FEA) was used to predict the magnitude and distribution of the von Mises stress on the coronoid process at the adductor insertion. HH33 mandibles from duck and quail were serially sectioned (10 μm thickness), stained with Milligan's trichrome, and imaged at 2.5× magnification. Images were aligned using the orbit and Meckel's cartilage as landmarks. Meckel's, the quadrate, surangular, and the mandibular adductor were manually segmented and reconstructed in 3D (Amira 6; FEI, Hillsboro, OR). The resulting 3D reconstructions of the jaw complexes were imported into commercial FEA software (ANSYS 17; Canonsburg, PA), which was used for meshing and analysis. Tissues were meshed using tetrahedral elements, which were sized based on convergence results from an iterative mesh refinement procedure. Final models utilized

178,378 (duck) and 54,954 elements (quail). The material properties calculated by Tanck et al. (2000) for mineralized embryonic mouse metatarsals (Young's Modulus (E) = 117 MPa; Poisson's Ratio (ν) = 0.3) were used for the surangular and Meckel's. The other structures were suppressed prior to performing FEA. Boundary conditions were prescribed to mimic those arising during jaw gaping, and included: 1) a fixed support at the contact surface between Meckel's and the quadrate; and 2) tensile force (duck 3.28E-04 N; quail 1.05E-04 N) aligned with the longitudinal axis of the mandibular adductor. The magnitudes of the adductor forces were determined using cross-sectional area measurements performed at the longitudinal midpoints and an assumed tensile stress of 1.11kPa (Landmesser and Morris, 1975). Statistical significance was determined using an unpaired, two-tailed, *t*-test (Prism 7, GraphPad).

2.10. Embryo paralysis

HH32 or HH33 duck were paralyzed using 10 mg/ml decamethonium bromide (DMBr) (Sigma-Aldrich, St. Louis, MO) in Hank's Buffered Sterile Saline (HBSS) and filter sterilized using a 0.22 μm filter. Each embryo was treated with a 0.5 ml dose of the DMBr solution administered as previously described (Hall, 1986; Solem et al., 2011).

2.11. Microdissections, RNA extraction, RT-qPCR, and analysis

Mandibular adductor insertions were dissected from paralyzed and control duck embryos at HH33 and HH36 and snap frozen in 70% EtOH mixed with dry ice. Microdissected samples were homogenized using a bead-mill (Omni International, Kennesaw, Kentucky) and RNA was isolated using the ARCTURUS PicoPure RNA Isolation Kit (ThermoFisher, Waltham, MA). 200 ng cDNA libraries were generated from RNA samples using iScript reverse transcriptase (BioRad, Hercules, CA). Each cDNA library was subsequently diluted to 2 ng/μl. Duck *Myod1*, *Sox9*, *TN-C*, and *Uch-L1* primer pairs were used to determine the relative enrichment of muscle, cartilage, tendon, and nerve tissues, respectively, relative to cDNA libraries from duck jaw complexes (Table S1). For quality control, HH33 cDNA libraries were excluded from analysis if the sample was enriched for muscle (> 1-fold enrichment of *Myod1* over control cDNA libraries), nerve (> 1.5-fold enrichment of *Uch-L1* over control cDNA libraries), or tendon (> 2.5-fold enrichment of *Sox9* over control cDNA libraries). At HH36, the top six tendon enriched samples with less than 4-fold *Myod1* enrichment were included in the analyses. *Fgf2*, *Fgf4*, *Fgf8*, *Fgfr1*, *Fgfr2*, *Fgfr3*, *Pea3*, *Erm*, *Tgfβ2*, *Tgfβ3*, *Tgfβr1*, *Tgfβr2*, *Tgfβr3*, *Smad3*, *Smad7b*, and *Pai1* expression was quantified by RT-qPCR using duck-specific primer pairs (Table S1). For all genes, expression was normalized to *β-Actin* and analysis was done following the ΔΔC(t) method (Ealba and Schneider, 2013; Livak and Schmittgen, 2001). P-values for − ΔΔC(t) values were calculated using an unpaired, two-tailed, Holm-Sidak test adjusted for multiple comparisons (Prism 7, GraphPad).

2.12. Generation of chimeras

GFP-chick (Crystal Bioscience, Emeryville, CA) and white Pekin duck eggs were incubated to HH9. Tungsten needles and Spemann pipettes were used to graft two differently sized populations of presumptive NCM along the midbrain and anterior hindbrain of chick donors into stage-matched duck hosts, producing chimeric "chuck" (Fish and Schneider, 2014a;

Fish et al., 2014; Merrill et al., 2008; Schneider, 1999; Schneider and Helms, 2003; Tucker and Lumsden, 2004). Small grafts of presumptive NCM (including neuroepithelium and overlying ectoderm) extended from the middle of the midbrain to the rostral hindbrain at rhombomere 2, whereas large grafts extended from the forebrain–midbrain boundary to rhombomere 2. Comparable-sized regions were excised from duck hosts. Orthotopic grafts and sham operations were performed as controls. Controls and chimeras were incubated side-by-side to ensure accurate staging during collections.

3. Results

3.1. Adult jaw morphology is presaged during embryonic development

There are many species-specific differences between Japanese quail and white Pekin duck mandibles. Quail mandibles are slender with a smooth coronoid process and diminutive retroarticular process (Fig. 1A). Duck mandibles feature a robust, laterally protruding coronoid process. Furthermore, duck mandibles are larger than quail, both absolutely and in relative proportion, and have a sizeable retro-articular process (Fig. 1B). Clearing and staining revealed that species-specific jaw morphology is established during embryonic development (Fig. 1C, D). At HH38, an elongate Meckel's cartilage is surrounded by lower jawbones, and the retroarticular processes are largely comprised of cartilage, yet quail and duck morphologies are already distinguishable. The most obvious difference is a secondary cartilage intermediate within the mandibular adductor insertion along the surangular in duck. Such cartilage is visible in cleared and stained duck as early as HH36. We never observed secondary cartilage on the coronoid process of quail or chick embryos.

3.2. NCM patterns the mandibular adductor complex in a dose-dependent manner

Presumptive NCM transplanted from HH9 GFP-positive chick into stage-matched duck hosts transformed the morphology of the jaw and coronoid process (Fig. 1E, F, I, J). The extent of transformation and distribution of GFP-positive NCM-derived connective tissues depended upon donor graft size. Small presumptive NCM transplants resulted in a limited distribution of GFP-positive skeletal and connective tissues, and produced minor changes to the size and shape of the jaw skeleton, but not enough to affect secondary chondrogenesis (Fig. 1G, H). In contrast, large transplants resulted in extensively distributed GFP-positive skeletal and connective tissues, and transformed the jaw to become more chick-like, including the absence of a secondary cartilage on the donor side coronoid process (Fig. 1K, L).

3.3. The progression of embryonic jaw motility is similar in quail and duck

In ovo videos of embryonic jaw motility captured periodic jaw gaping in quail and duck embryos (Fig. 2A–D)(Movies S1, S2). The first quantifiable jaw movements occurred at HH33 in quail and duck. HH33 quail were active 10.46% of the time (95% CI ± 3.07%, n = 9) while stage-matched duck were active 5.2% of the time (95% CI ± 1.06%, n = 10). Both the frequency and duration of jaw movements increased with developmental time in quail and duck (Fig. 2E, F). Quail and duck jaw motility tracked closely at HH34 (18.82% ± 8.32%, n = 12 for quail and 15.72% ± 3.28%, n = 18 for duck) and HH35 (28.58% ± 16.63%, n = 6 for quail and 29.35% ± 6.57%, n = 2 for duck). No statistically significant

differences in motility were observed in developmental stages preceding the appearance of secondary cartilage. A significant difference was observed at HH36 (26.66% ± 8.36%, n = 22 for quail, and 43.97% ± 5.06, n = 26 for duck, $p < 0.0005$), however, by this stage, a secondary cartilage was already formed on the coronoid process. Peak quail jaw motility was observed at HH37 (67.39% ± 5.7%, n = 6 in quail, versus 51.72% ± 8.69%, n = 13 in duck) while duck motility peaked at HH38, but did not exceed quail motility (60.76% ± 5.79%, n = 7 in duck versus 61.67% ± 5.49%, n = 7 in quail).

Supplementary material related to this article can be found online at doi:10.1016/j.ydbio.2018.05.002.

3.4. FEA predicts distinct mechanical environments at the quail and duck coronoid process

3D reconstructions of HH33 quail and duck jaws including Meckel's, the quadrate, postorbital, surangular, and mandibular adductor were created by manually segmenting histological images (Fig. 3A, B). Reconstructions revealed species-specific, geometrical differences in cross-sectional area of the muscle, direction of contractile force, and area of the surangular over which force is applied. In duck, the mandibular adductor inserts on the lateral aspect of the surangular, while in quail, the insertion is dorsal. In duck, the insertion is also more proximal to the jaw joint. At its widest, the cross-sectional area of the duck mandibular adductor is 321,000 μm^2, while the slender quail muscle is only 114,192 μm^2 indicating that maximum contractile force of the duck muscle is roughly 2.8 times greater than quail.

Finite element models of the insertion site between the mandibular adductor and the surangular predicted that duck experience a maximum shear stress concentration roughly 60 times greater than quail (0.96 MPa in duck versus 0.016 MPa in quail)(Fig. 3C, D). Furthermore, the mean von Mises stress experienced in duck (0.053 MPa) is significantly higher than in quail (0.0045 MPa; $p < 0.0001$). Histograms also revealed the state of shear stress at the insertion is more homogeneous in quail, while tissue at the duck insertion is subjected to a broader range of shear stress (Fig. 3E).

3.5. The FGF pathway changes during development and is affected by paralysis

RT-qPCR analyses on microdissected duck mandibular adductor insertions revealed significant increases in ligands *Fgf2* (5.34 ± 1.50-fold change, $p < 0.0005$), *Fgf4* (449.89 ± 237.59-fold change, $p < 0.0005$), and *Fgf8* (56.22 ± 44.55-fold change, $p < 0.0005$) from HH33 to HH36 (n = 13 for HH33 controls, n = 10 for HH36 con-trols)(Fig. 4A). FGF receptors *Fgfr1* (0.76 ± 0.21-fold change, $p < 0.05$), *Fgfr2* (0.19 ± 0.18-fold change, $p < 0.0005$), and *Fgfr3* (0.68 ± 0.30-fold change, $p < 0.05$) significantly diminished in expression over this time. Transcriptional effectors *Pea3* (5.61 ± 1.09-fold change, $p < 0.0005$) and *Erm* (2.44 ± 0.54-fold change, $p < 0.0005$) were both significantly more abundant at HH36 than at HH33.

Paralysis at HH32 did not result in significant changes to FGF signaling pathway members or effectors at HH33 relative to stage-matched controls. In HH36 paralyzed embryos, the only FGF ligand with a significant increase was *Fgf2* in comparison to HH33 controls (3.67

± 1.30-fold change, $p < 0.0005$) (n = 12 for HH33 paralyzed, n = 11 for HH36 paralyzed). However, in HH36 paralyzed embryos, *Fgf2* was still significantly less in abundant than in stage-matched controls ($p < 0.05$) (asterisk, Fig. 4A). In paralyzed HH36 embryos, *Fgf4* was 21.49 ± 33.68-fold more abundant than in HH33 controls and *Fgf8* was 4.79 ± 5.06-fold more abundant, but both genes were still significantly less expressed than in stage-matched controls ($p < 0.005$ for both)(asterisks, Fig. 4A). At HH36, *Fgfr1* (0.55 ± 0.22-fold change, $p < 0.0005$) and *Fgfr2* (0.35 ± 0.29-fold change, $p < 0.0005$) were significantly down in paralyzed samples, similar to expression dynamics seen in controls over the same period. Unlike control samples, *Pea3* (2.58 ± 2.75-fold change) and *Erm* (1.49 ± 0.67-fold change) remained relatively flat in paralyzed embryos and, by HH36, were significantly less abundant than in HH36 controls ($p < 0.05$ for both) (asterisks, Fig. 4A).

Analysis of spatial and temporal gene expression patterns was conducted in control and paralyzed duck at HH33 and HH36 (Table 1). At HH33, in sagittal section, the mandibular adductor was visible as two muscle bundles divided proximodistally by the mandibular branch of the trigeminal nerve (Fig. 4B). Proximal to the mandibular nerve, the mandibular adductor appeared fan-like and inserted broadly. Distal to the nerve, unipinnate muscle fibers were joined by a fibrous aponeurosis. The musculature and aponeurosis appeared relatively disorganized following 24 h of paralysis (Fig. 4F).

At HH33, *Fgf4* was expressed throughout primary cartilages like the quadrate, and Meckel's, as well as in skeletal muscles like the mandibular adductor, the mandibular adductor insertion, and the mesenchymal condensation that would give rise to secondary cartilage (n = 5 for each gene)(Fig. 4C). After 24 h of paralysis, *Fgf4* was maintained in the quadrate and Meckel's, but diminished in the mandibular adductor and its insertion (Fig. 4G). *Fgf8* was in the mandibular adductor, the mandibular adductor insertion, the secondary cartilage insertion, and the surangular condensation (Fig. S1). There was also *Fgf8* in primary cartilages like Meckel's and the quadrate. The secondary cartilage condensation and its *Fgf8* domain were not present in embryos 24 h after paralysis (Fig. S1). *Fgfr2* was in the quadrate and Meckel's, particularly in the perichondrium, as well as in the secondary cartilage condensation and the nascent surangular (Fig. 4D). Following 24 h of paralysis, expression in primary cartilage was maintained, while expression in the secondary cartilage condensation and surangular condensation were diminished (Fig. 4H). *Fgfr3* was in the quadrate and Meckel's, but not perichondria, and in the surangular condensation with greater expression around the periphery (Fig. 4E). Paralysis led to decreased expression in the surangular condensation while expression in primary cartilage was maintained (Fig. 4I). *Pea3* was in the mandibular adductor, the mandibular adductor insertion, and the secondary cartilage condensation (Fig. S1). There was also expression in the surangular condensation, primary cartilages, and perichondria. 24 h after paralysis, the secondary cartilage condensation failed to form and the corresponding region of *Pea3* was absent (Fig. S1).

By HH36, secondary cartilage was encapsulated by a dense fibrous sheath within the mandibular adductor insertion (i.e., enthesis) and separate from the periosteum of the surangular bone (Fig. 4J). The mandibular adductor muscles began to separate into distinct superficial sheet-like, proximal fan-like, and distal groups of fibers. HH36 paralyzed

embryos had poor muscle and tendon organisation and lacked a secondary cartilage condensation (Fig. 4N). *Fgf4* (n = 5 for each gene) was strongly expressed at HH36 in the mandibular adductor, the mandibular adductor insertion, and the surangular and periostea (Fig. 4K). The quadrate and Meckel's also expressed *Fgf4* throughout the cartilage and perichondrium. *Fgf4* was also seen within the secondary cartilage condensation. Paralysis prevented secondary chondrogenesis, however, *Fgf4* was maintained in muscle, bone, and primary cartilages (Fig. 4O). *Fgf8* was in the mandibular adductor, tendon, and secondary cartilage (Fig. S1). *Fgf8* was also in the surangular, periosteum, and primary cartilage. Paralysis prevented secondary cartilage from forming, but *Fgf8* was still in muscle and its connective tissues (Fig. S1). *Fgfr2* was in muscle, tendon, bone, periostea, cartilage, perichondria, and within secondary cartilage (Fig. 4L). Following paralysis, the only change to *Fgfr2* was the absence of a secondary cartilage domain (Fig. 4P). *Fgfr3* was in the quadrate and Meckel's as well as in the periosteum of the surangular. *Fgfr3* was also in muscle, tendon, bone, periostea, cartilage, perichondria, and secondary cartilage (Fig. 4M). Expression in the secondary cartilage was highest at the center and became lower towards the periphery. In paralyzed embryos, only the *Fgfr3* domain in secondary cartilage was absent (Fig. 4Q). *Pea3* was in the mandibular adductor muscle, tendon, and the secondary cartilage condensation (Fig. S1). *Pea3* was also in primary cartilage, perichondria, bone, and periostea. As secondary cartilage failed to form in HH36 paralyzed embryos, *Pea3* was absent (Fig. S1).

3.6. The TGFβ pathway changes during development and is affected by paralysis

Quantitative RT-PCR showed that *Tgfβ2* (4.28 ± 1.29-fold change, $p < 0.0005$) and *Tgfβ3* (7.19 ± 2.11-fold change, $p < 0.0005$) increased significantly from HH33 to HH36 (n = 10 for HH33 controls, n = 10 for HH36 controls) (Fig. 5A). Paralyzed embryos mirrored the increases in *Tgfβ2* (2.87 ± 1.36-fold change, $p < 0.05$) and *Tgfβ3* (5.50 ± 2.30-fold change, $p < 0.0005$) over the same period. Transcriptional activity of receptors *Tgfβr1*, *Tgfβr2*, *Tgfβr3*, and transcriptional effectors *Smad3*, *Smad7b*, and *Pai1* remained flat in controls. In contrast, HH36 paralyzed samples expressed more *Pai1* (2.53 ± 1.89-fold change) than HH33 controls ($p < 0.05$), and achieved significantly greater expression than HH36 control samples ($p < 0.05$) (asterisk, Fig. 5A).

Our qualitative analyses showed that at HH33, *Tgfβ2* was expressed in the mandibular adductor muscle, the mandibular adductor insertion, and the secondary cartilage condensation (Fig. 5B, C). At HH33, following 24 h of paralysis, expression in muscle and tendon persisted while the secondary cartilage condensation and its *Tgfβ2* domain did not (Fig. 5F, G). *Tgfβ3* was also in the mandibular adductor muscle, the mandibular adductor insertion, primary cartilage like Meckel's and the quadrate, and the secondary cartilage condensation (Fig. 5D). At this stage, the only *Tgfβ3* domain affected by paralysis was in the secondary cartilage condensation (Fig. 5H). *Tgfβr2* was in the mandibular adductor, the mandibular adductor insertion, and in the secondary cartilage condensation (Fig. 5E). *Tgfβr2* was also in Meckel's and the quadrate. Following paralysis, the only expression domain affected was the secondary cartilage condensation (Fig. 5I). *Smad3* was in the mandibular adductor, the insertion, and the secondary cartilage condensation (Fig. S1). *Smad3* was also

in the quadrate, Meckel's, and other primary cartilages. The secondary cartilage domain did not appear in stage-matched, paralyzed embryos (Fig. S1).

In HH36 duck, *Tgfβ2* was in muscles like the mandibular adductor, tendons like the mandibular adductor insertion, bones like the surangular and their periostea, and cartilages like Meckel's, the quadrate, and their perichondria (Fig. 5K). *Tgfβ2* was also expressed throughout the secondary cartilage on the coronoid process. Following paralysis, the only change in expression at HH36 was for *Tgfβ2* coincident with the loss of secondary cartilage (Fig. 5O). *Tgfβ3* was in all the same tissues as *Tgfβ2* in HH36 control and paralyzed embryos, including the secondary cartilage (Fig. 5L, P). By HH36, *Tgfβr2* was in the surangular, as well as secondary cartilage on the coronoid process (Fig. 5M). Following paralysis, the secondary cartilage and its *Tgfβr2* domain were absent while *Tgfβr2* was unaffected in bone (Fig. 5Q). *Smad3* was in the mandibular adductor and its insertion, and in the secondary cartilage. There was also *Smad3* in primary cartilages, perichondria, bone, and periostea (Fig. S1). Paralyzed HH36 embryos did not form secondary cartilage so the corresponding *Smad3* expression was absent (Fig. S1).

3.7. Inhibiting FGF or TGFβ signaling affects the condensation of secondary cartilage

Unilateral delivery of FGF signaling inhibitor SU5402 blocked the formation of, or reduced the size of secondary cartilage on the coronoid process (n = 18 at HH32, n = 29 at HH33) (Fig. 6A,C). No change in secondary cartilage was observed following delivery of DMSO control beads (n = 6). The efficacy of secondary cartilage inhibition at HH38 depended upon the stage of treatment, with HH32 embryos being more sensitive to FGF inhibition than HH33 embryos (Fisher's exact test, p = 0.0047). In 88.9% of embryos treated with SU5402 at HH32, secondary cartilage was either lost or reduced in size (n = 16/18). Of those secondary cartilage phenotypes, 50% were reduced in size (n = 8/16), and 50% had a complete absence (n = 8/16) of secondary cartilage. FGF inhibition at HH33 reduced the size of the secondary cartilage in 31.01% of cases (n = 9/29) and prevented secondary cartilage induction in 13.79% of cases (n = 4/29).

Inhibition of TGFβ signaling by delivering SB431542 also frequently caused loss or reduction in the size of the secondary cartilage on the coronoid process (n = 37 at HH32, n = 66 at HH33)(Fig. 6B, D). Although the statistical distribution of outcomes did not depend on whether embryos were treated at HH32 (40.54% absent or reduced secondary cartilage, n = 15/37) or HH33 (39.39% absent or reduced secondary cartilage, n = 26/66), HH32 treatments tended to be more efficacious at preventing secondary chondrogenesis (13.51%, n = 5/37) than HH33 treatments (3.03%, n = 2/66).

3.8. Inhibiting FGF or TGFβ signaling does not lead to increased cell death

TUNEL staining showed that implanting AG1X2 chromatography beads soaked in DMSO (n = 3 embryos) or small molecule inhibitors of FGF signaling (n = 6 embryos) or TGFβ signaling (n = 7 embryos) at HH32 did not increase cell death nor did we observe histological evidence at any stage where muscle or tendon formation were blocked by treatment delivery (data not shown). 24 h after implantation, 0.69% of cells surrounding DMSO soaked beads were undergoing apoptosis (n = 5 sections) (Fig. 6E, F). There was

no significant increase in cell death over control beads with SU5402 (1.42%, n = 19 sections) or SB431542 (0.22%, n = 29 sections) (Fig. 6H, I) treatments. For comparison, DNase-treated positive control slides showed significantly more cell death (52.60%, n = 3 sections, unpaired *t*-test $p < 0.0001$) (Fig. 6G).

3.9. Exogenous FGF and TGFβ treatments can restore cartilage in paralyzed embryos

HH38 duck embryos paralyzed and treated with FGF4 beads at HH32 formed cartilage adjacent to or surrounding the bead in 27.27% of cases (n = 3/11) (Fig. 7B). No cartilage was induced in any embryos treated with BSA beads alone (n = 4 heparin acrylic, n = 12 Affigel blue) (asterisk, Fig. 7A), or in cases where recombinant protein soaked beads were located outside the region of the mandibular adductor insertion (n = 4 for FGF4, n = 2 for TGFβ2/TGFβ3, and n = 4 for FGF4/TGFβ2/TGFβ3). Paralysis and implantation of beads soaked in TGFβ2 and TGFβ3 induced cartilage in 75% of HH38 duck (n = 15/20) (Fig. 7C). Implanting both FGF4 and TGFβ2/TGFβ3 soaked beads in paralyzed HH32 duck induced cartilage in 85.71% of cases (n = 12/14) (Fig. 7D). Treating HH32 quail with exogenous TGFβ2/TGFβ3 induced a chondrogenic response in 11.11% of embryos (n = 1/9) (Fig. 7E). Safranin-O staining confirmed the presence of a glycosaminoglycan-rich cartilaginous extracellular-matrix surrounding the beads (n = 2/3) (Fig. 7F). Although spherical beads were implanted, the axial orientation of Safranin-O-positive tissue surrounding the beads was not radially symmetrical and tended to align with the orientation of the mandibular adductor insertion. Analysis of paralyzed duck rescue experiments revealed that the distribution of phenotypes depended upon the ligand or ligands received (Fisher's Exact Test, $p = 0.005$) (Fig. 7G).

4. Discussion

4.1. NCM controls the species-specific pattern of the mandibular adductor insertion

In previous studies we showed that NCM controls the species-specific size and shape of the jaw skeleton and associated musculature via cell-autonomous morphogenetic programs (Solem et al., 2011; Tokita and Schneider, 2009). In the present study, we expanded these findings and substantiated that this patterning ability is dose-dependent. While we know that the extent of gene expression in chimeras is directly related to the degree of chimerism (Ealba and Schneider, 2013), we extended this principle to morphology and modulated the presence or absence of secondary cartilage on the coronoid process by titrating the size of presumptive NCM transplants and thus the distribution of NCM-derived connective tissues. Small transplants did not alter secondary cartilage development whereas larger transplants did. Based on our prior analyses of muscle and connective tissue patterning (Solem et al., 2011; Tokita and Schneider, 2009), and the known critical role for interactions between NCM and muscle pre-cursors (Bothe et al., 2007; Evans and Noden, 2006; Grenier et al., 2009; Noden, 1983, 1988; Noden and Trainor, 2005; Rinon et al., 2007), we expect that increasingly larger populations of donor presumptive NCM relocate the mandibular adductor insertion from a duck-like lateral position to one that is more dorsal and chick-like. In this way, and concomitant with its patterning abilities, NCM would be acting as a major determinant of the mechanical environment whereby specific loading conditions are more conducive to secondary cartilage formation.

4.2. Quality not quantity of mechanical stimulation drives secondary chondrogenesis

Secondary cartilage development can be divided into two phases: induction and maintenance. Both phases require proper biomechanical stimulation. Developmental plasticity is the conduit through which embryonic motility influences morphogenesis (Anthwal et al., 2015; Blitz et al., 2009; Brunt et al., 2017; Carter and Beaupré, 2007; Hall, 1967, 1968, 1972, 1986; Hall and Herring, 1990; Havis et al., 2016; Huang et al., 2013; Kardon, 1998; Pitsillides, 2006; Pollard et al., 2014; Schweitzer et al., 2010; Sharir et al., 2011; Shwartz et al., 2012; Solem et al., 2011; Wu et al., 2001) and ultimately allows embryonic form to presage adult function. For induction of secondary cartilage to occur, the frequency of mechanical stimulation must cross a threshold (Hall, 1967, 1968). The similarity in early quail and duck jaw motility indicates that frequency of jaw activity is an unlikely determinant of species-specific secondary chondrogenesis. A significant difference in motility manifests at HH36, but, by that time, the duck coronoid process has already established a secondary cartilage. Thus, we conclude that the frequency of mechanical stimulation is not, itself, sufficient to induce secondary cartilage in quail versus duck. We favor a model in which secondary cartilage is induced by biomechanical stresses resulting from a combination of species-specific muscle pattern and resultant differences in the quality or type of functional loading on the muscle insertion.

4.3. Mechanical cues result from and contribute to species-specific morphology

Prior work has highlighted the contribution of the mechanical environment in wrap-around and other force-transmitting tendons (Benjamin and Ralphs, 1998; Blitz et al., 2013; Carter and Beaupré, 2007; Murchison et al., 2007; Schweitzer et al., 2010; Shwartz et al., 2013). Such a configuration, in which a tendon experiences not only axial tension but also compression against the surface of the bone, is conducive to fibrocartilage development (Blitz et al., 2009; Koo et al., 2017). Thus, the evolutionary presence or absence of secondary cartilage on the coronoid process reflects species-specific variation in functional anatomy determined by in ovo mechanical loading (Beresford, 1981; Fang and Hall, 1997; Hall, 1979; Stutzmann and Petrovic, 1975). In taxa such as humans, rats, cats, and duck, secondary cartilage forms at the jaw adductor muscle insertion (Amorim et al., 2010, 2008; Hall, 2005; Horowitz and Shapiro, 1951; Kantomaa and Rönning, 1997; Moore, 1973, 1981; Solem et al., 2011; Soni and Malloy, 1974; Vinkka, 1982; Washburn, 1947) whereas an equivalent secondary cartilage is absent in mice, guinea pigs, chick, and quail (Anthwal et al., 2008, 2015; Boyd et al., 1967; Moss and Meehan, 1970; Rot-Nikcevic et al., 2007; Shibata et al., 2003; Solem et al., 2011). Our work implies that the reason secondary cartilage forms at this location in some species and not others is due to the way embryonic motility interacts with NCM-mediated muscle pattern to create differential forces.

To our knowledge, this is one of the first finite element models presented for the embryonic jaw adductor complex. Our FEA illuminates species-specific differences in both the predicted magnitude and spatial distribution of von Mises stress in the mandibular adductor insertion prior to secondary chondrogenesis. Perhaps the wide ranging magnitudes of shear stress distributed across the surface of the duck surangular mediates the precise, spatially restricted formation of secondary cartilage. Post-hatching, the secondary cartilage eventually ossifies and becomes continuous with the surangular bone (Coues, 1887; Dawson

et al., 2011; Mitgutsch et al., 2011; Zweers et al., 1977a, 1977b). The resulting structure distinguishes both the form and the functional mechanics of adult duck versus quail jaw complexes. However, the mechanisms that facilitate the relationship between mechanical stimulation and musculoskeletal adaptation have remained largely unknown.

While previous studies have implicated FGF and TGFβ signaling in both early, muscle-independent, and late, muscle-dependent, phases of sclerotome-derived limb tendons (Havis et al., 2016, 2014; Huang et al., 2015), our findings suggest that mechanical cues drive differential activation of FGF and TGFβ signaling to induce species-specific secondary cartilage within an NCM-derived tendon insertion. Moreover, we do not observe any evidence for crosstalk between these pathways, given that paralysis downregulates FGF signaling while TGFβ expression remains unchanged. Conversely, despite the maintenance of TGFβ, FGF is downregulated. Such findings are consistent with the independent functions of these pathways during chick limb tendon morphogenesis (Havis et al., 2016). However, manipulating these pathways in the limb does not induce cartilage formation.

4.4. FGF and TGFβ are necessary and sufficient for secondary chondrogenesis

Molecular programs of tendon development are context-dependent. In mouse limbs, TGFβ signaling promotes tendon development while FGF signaling is inhibitory (Blitz et al., 2013; Havis et al., 2014; Pryce et al., 2009; Subramanian and Schilling, 2015). However, FGF signaling is a pro-tendon signal in chick limbs and promotes axial mouse and chick tendon development (Brent et al., 2005, 2003; Edom-Vovard et al., 2001, 2002; Havis et al., 2016, 2014; Smith et al., 2005). Our quantitative and qualitative analyses demonstrated that FGF and TGFβ pathway members are expressed in musculoskeletal tissues throughout secondary cartilage induction and maintenance, and paralysis significantly but differentially affected transcription of many of these genes. We found that paralysis dramatically downregulated *Fgf4* and *Fgf8*, indicating that their expression may be mediated by mechanical stimulation. Furthermore, FGF signaling activity decreased following paralysis as indicated by the relative down regulation of *Pea3* and *Erm* transcription. While the role of FGF signaling in the context of cartilage, bone, muscle, and limb tendon is well described (Brent et al., 2005; Edom-Vovard et al., 2001; Eloy-Trinquet et al., 2009; Murakami et al., 2000; Ornitz and Marie, 2015), the influence of the mechanical environment on FGF signaling remains unclear. While paralysis did not affect transcription of TGFβ ligands or receptors, the downstream effector *Pai1* (Kawarada et al., 2016) was significantly increased by paralysis, suggesting tissue atrophy and fibrosis in response to disuse (Naderi et al., 2009). TGFβ signaling is responsive to the mechanical environment (Kleinnulend et al., 1995; Nguyen et al., 2013; Robbins et al., 1997; Shi et al., 2011), but how mechanical cues exert control over TGFβ signaling is not as well understood. Our results suggest that, in this context, TGFβ signaling activity is primarily regulated by post-transcriptional modifications like phosphorylation of SMADs (Anthwal et al., 2008; Berthet et al., 2013; Maeda et al., 2011; Wipff et al., 2007) and regulation of free, active TGFβ ligands.

Tgfβ2 null mice and conditional *Tgfβr2* knockout mice develop malformations of the dentary and its coronoid, condylar, and angular processes (Oka et al., 2008, 2007; Sanford et al., 1997), although, the defects of the three processes likely arise via different

developmental mechanisms. Mice, unlike duck and human, do not form the coronoid process via a secondary cartilage intermediate. In *Tgfβ2* null mice, the condylar and angular processes are smaller, but the secondary cartilages on these processes persist. However, secondary chondrogenesis was prevented by conditional *Tgfβr2* knockout in neural crest derived cells. Mandible culture experiments in mice also demonstrated that TGFβ signaling is required for condylar and angular secondary cartilage induction (Anthwal et al., 2008). In the context of our experiments, TGFβ inhibition did not produce bone defects, nor did we observe abnormalities in Meckel's. This is consistent with *Tgfβ2*, *Tgfβ3*, and limb specific *Tgfβr2* knockout data in which limb tendon formation is severely inhibited while primary cartilage is largely unperturbed (Pryce et al., 2009).

Our paralysis rescue experiments led to the formation of a dense fibrous capsule and even cartilage around the bead. Although ligands were delivered using spherical beads and presumably diffused uniformly (Eichele et al., 1984), the axis of Alcian blue or Safranin-O positive tissue surrounding the beads was not radially symmetrical, suggesting that the mesenchyme and surrounding connective tissues overlying the surangular are not all equivalent in their capacity to generate secondary cartilage. Furthermore, the locations where cartilage was induced were spatially restricted to the general region where secondary cartilage forms in controls. In duck and quail, beads implanted too distal from the jaw joint, or too superficial, superior, or inferior to the surangular did not elicit a chondrogenic response. The FGF and TGFβ signaling-dependent chondrogenic response we observed in quail and duck may be localized to tendon and connective tissues surrounding the mandibular adductor insertion. Such a spatial constraint parallels published explant data in which the murine coronoid process, which does not ordinarily form a secondary cartilage, can be induced to do so by fetal bovine serum (FBS Anthwal et al., 2015). Though FBS bathed the entire mandible, ectopic cartilage was only observed on the coronoid process. Other experiments on developing limb tendons corroborate the ability of exogenous FGF and TGFβ ligands to maintain *Scx* even in the absence of mechanical stimulation, but to our knowledge, no instances of induced cartilage have been reported in those contexts (Edom-Vovard et al., 2002; Havis et al., 2016).

In our experiments, induced cartilage appears to be encapsulated and distinct from the periosteum of surangular bone, mirroring native secondary cartilage development on the duck coronoid process. Thus, the secondary cartilage on the coronoid process is likely derived from cells in the tendon and adjacent connective tissue, not the periosteum as in articular secondary cartilage (Buxton et al., 2003). Experiments in other contexts suggest the existence of progenitor cells that express both tendon (e.g., *Scx, Tcf4*) and cartilage (e.g., *Sox9*) tissue markers that establish and contribute to certain sites where tendons or ligaments insert onto primary cartilage (Blitz et al., 2013; Kardon, 1998; Kardon et al., 2003; Mathew et al., 2011; Schweitzer et al., 2001; Sugimoto et al., 2013). Our previous analyses support the idea that cells expressing a similar set of lineage markers may give rise to secondary cartilage on the coronoid process since it forms within a tendon (Solem et al., 2011; Tokita and Schneider, 2009).

4.5. Mechanical cues differentially regulate members of the FGF and TGFβ pathways

Clearly, musculoskeletal development and homeostasis depend upon proper biomechanical cues, however, the cell-biology that mediates mechanosensation is not well understood. A variety of mechanisms including the primary cilium, Wnt signaling, and especially sclerostin, which is an osteocyte-specific Wnt inhibitor, have been implicated in mechanosensitive bone remodeling (Robling et al., 2016, 2008; Rolfe et al., 2014; Tu et al., 2012). Other potential mechanisms include ligands being freed from the extracellular matrix, ion channels, focal adhesions, cytoskeletal dynamics, and many others (del Rio et al., 2009; Dupont et al., 2011; Hamill and McBride, 1996; Maeda et al., 2011; Mammoto and Ingber, 2010; Matthews et al., 2006; McBeath et al., 2004; Pruitt et al., 2014; Quinn et al., 2002; Raizman et al., 2010; Ramage et al., 2009; Roberts et al., 2001; Shakibaei and Mobasheri, 2003; Solem et al., 2011; Vincent et al., 2002, 2007; Wang et al., 2009; Wen et al., 2017).

From our qualitative and quantitative analyses, a subset of genes stood out as likely mediating development of the mandibular adductor complex (*Tgfβ2, Tgfβ3, Fgfr1*, and *Fgfr2*) as their abundance changed significantly and in the same direction regardless of whether the embryo was paralyzed or not. This group of genes includes *Tgfβ2* and *Tgfβ3*, which both rescued cartilage formation when delivered as ligands to paralyzed duck or normal quail embryos, suggesting that TGFβ signaling activity may be modulated post-transcriptionally. For example, secondary chondrogenesis may depend upon the availability of free, active TGFβ ligands. Also, we observed no change in *Tgfβr1*, *Tgfβr2*, *Tgfβr3*, *Smad3*, or *Smad7b* expression though *Pai1* was significantly more abundant in paralyzed samples. These data support the hypothesis that TGFβ pathway-mediated responses to mechanical stimulation utilize post-transcriptional mechanisms, which is something we will test in future studies.

Our analyses also indicate that a set of five FGF signaling pathway components (*Fgf2*, *Fgf4, Fgf8, Pea3*, and *Erm*) likely depends upon embryonic muscle contraction to maintain expression and mediate secondary chondrogenesis. FGF signaling has been implicated in other mechanosensitive processes (Vincent et al., 2002, 2007; Wen et al., 2017), but there is still a lot to learn about how FGF ligands, receptors, and transcriptional effectors interact with the mechanical environment.

Our data suggest a model (Fig. 8) whereby species-specific secondary chondrogenesis on the coronoid process arises from functional motility acting upon NCM-derived form. In our model, the stress within the mandibular adductor insertion differentially activates FGF and TGFβ signaling, thereby inducing secondary chondrogenesis. Consequently, biomechanical cues modulate cell-autonomous, developmental programs to generate species-specific jaw geometry and promote structural and functional integration of the musculoskeletal system during development.

Russell (1916), in his classic book, *Form and Function*, posed the question, “Is function the mechanical result of form, or is form merely the manifestation of function or activity? What is the essence of life, organisation or activity? (p.v)” Our findings provide evidence that form initially dictates function but then function modulates form. Cranial NCM establishes

species-specific “organisation” prior to the onset of muscle “activity.” However, as jaw activity begins, form adapts to support functional demands. In duck, species-specific form, coupled with jaw activity, creates mechanical stresses that differentially activate FGF and TGFβ signaling to induce secondary cartilage formation on the coronoid process. Our data highlight the role of NCM in not only mediating form but also in shaping the biomechanical environment. Furthermore, plasticity in neural crest-derived tissues enables seamless integration of form and function during embryonic development, adult homeostasis, and evolution. Likewise, these same mechanisms likely go awry following injury or in disease.

Supplementary Material

Refer to Web version on PubMed Central for supplementary material.

Acknowledgments

We thank J. Lotz, T. Alliston, R. Marcucio, J. Fish, and members of the Schneider lab for helpful discussions; Z. Vavrusova, M. Bodendorfer (Hague), D. Jaul, M. Chung, S. Smith, and D. Chu for technical assistance; the Biological Imaging Development Center at UCSF for data analysis software; and T. Dam at AA Lab Eggs for quail and duck eggs. This work was supported in part by NICHD T32 HD007470 and F31 DE024405 to K.C.W.; and NIDCR R01 DE016402, R01 DE025668, and S10 OD021664 to R.A.S.

Appendix A. Supplementary material

Supplementary data associated with this article can be found in the online version at doi:10.1016/j.ydbio.2018.05.002.

References

Albrecht U, Eichele G, Helms JA, Lu HC. 1997 Visualization of gene expression patterns by in situ hybridization. Mol Cell Methods Dev Toxicol. :23–48.

Ainsworth SJ, Stanley RL, Evans DJ. 2010; Developmental stages of the Japanese quail. J Anat. 216 :3–15. [PubMed: 19929907]

Amorim MM, Borini CB, de Castro Lopes SL, de Oliveira Tosello D, Berzin F, Caria PH. 2010; Relationship between the angle of the coronoid process of the mandible and the electromyographic activity of the temporal muscle in skeletal class I and III individuals. J Oral Rehabil. 37 :596–603. [PubMed: 20529175]

Amorim MM, Borini CB, Lopes SL, Haiter-Neto F, Berzin F, Caria PH. 2008; Relationship between the inclination of the coronoid process of the mandible and the electromyographic activity of the temporal muscle in skeletal class I and II individuals. J Oral Sci. 50 :293–299. [PubMed: 18818465]

Anthwal N, Chai Y, Tucker AS. 2008; The role of transforming growth factor-beta signalling in the patterning of the proximal processes of the murine dentary. Dev Dyn. 237 :1604–1613. [PubMed: 18498113]

Anthwal N, Peters H, Tucker AS. 2015; Species-specific modifications of mandible shape reveal independent mechanisms for growth and initiation of the coronoid. Evodevo. 6

Balooch G, Balooch M, Nalla RK, Schilling S, Filvaroff EH, Marshall GW, Marshall SJ, Ritchie RO, Derynck R, Alliston T. 2005; TGF-beta regulates the mechanical properties and composition of bone matrix. Proc Natl Acad Sci USA. 102 :18813–18818. [PubMed: 16354837]

Baumel, JJ. Handbook of Avian Anatomy: Nomina Anatomica Avium. Nuttall Ornithological Club; Cambridge, Mass: 1993.

Benjamin M, Ralphs JR. 1998; Fibrocartilage in tendons and ligaments–an adaptation to compressive load. J Anat. 193 (Pt 4) :481–494. [PubMed: 10029181]

Beresford, WA. Chondroid Bone, Secondary Cartilage, and Metaplasia. Urban & Schwarzenberg; Baltimore, MD: 1981.

Berthet E, Chen C, Butcher K, Schneider RA, Alliston T, Amirtharajah M. 2013; Smad3 binds scleraxis and mohawk and regulates tendon matrix organization. J Orthop Res. 31 :1475–1483. [PubMed: 23653374]

Blitz E, Sharir A, Akiyama H, Zelzer E. 2013; Tendon-bone attachment unit is formed modularly by a distinct pool of Scx- and Sox9-positive progenitors. Development. 140 :2680–2690. [PubMed: 23720048]

Blitz E, Viukov S, Sharir A, Shwartz Y, Galloway JL, Pryce BA, Johnson RL, Tabin CJ, Schweitzer R, Zelzer E. 2009; Bone ridge patterning during musculoskeletal assembly is mediated through SCX regulation of Bmp4 at the tendon-skeleton junction. Dev Cell. 17 :861–873. [PubMed: 20059955]

Bothe I, Ahmed MU, Winterbottom FL, von Scheven G, Dietrich S. 2007; Extrinsic versus intrinsic cues in avian paraxial mesoderm patterning and differentiation. Dev Dyn. 236 :2397–2409. [PubMed: 17654605]

Boyd TG, Castelli WA, Huelke DF. 1967; Removal of the temporalis muscle from its origin: effects on the size and shape of the coronoid process. J Dent Res. 46 :997–1001. [PubMed: 5248985]

Brent AE, Braun T, Tabin CJ. 2005; Genetic analysis of interactions between the somitic muscle, cartilage and tendon cell lineages during mouse development. Development. 132 :515–528. [PubMed: 15634692]

Brent AE, Schweitzer R, Tabin CJ. 2003; A somitic compartment of tendon progenitors. Cell. 113 :235–248. [PubMed: 12705871]

Brunt LH, Begg K, Kague E, Cross S, Hammond CL. 2017; Wnt signalling controls the response to mechanical loading during zebrafish joint development. Development. 144 :2798–2809. [PubMed: 28684625]

Buxton PG, Hall B, Archer CW, Francis-West P. 2003; Secondary chondrocyte-derived Ihh stimulates proliferation of periosteal cells during chick development. Development. 130 :4729–4739. [PubMed: 12925598]

Callahan JF, Burgess JL, Fornwald JA, Gaster LM, Harling JD, Harrington FP, Heer J, Kwon C, Lehr R, Mathur A, Olson BA, Weinstock J, Laping NJ. 2002; Identification of novel inhibitors of the transforming growth factor beta1 (TGF-beta1) type 1 receptor (ALK5). J Med Chem. 45 :999–1001. [PubMed: 11855979]

Carter, DR, Beaupré, GS. Skeletal Function and Form: Mechanobiology of Skeletal Development, Aging, and Regeneration. Cambridge University Press; Cambridge, UK: 2007.

Chamberlain, FW. Atlas of Avian Anatomy; Osteology, Arthrology, Myology. Michigan State College; East Lansing, Mich: 1943.

Chang JL, Brauer DS, Johnson J, Chen CG, Akil O, Balooch G, Humphrey MB, Chin EN, Porter AE, Butcher K, Ritchie RO, Schneider RA, Lalwani A, Derynck R, Marshall GW, Marshall SJ, Lustig L, Alliston T. 2010; Tissue-specific calibration of extracellular matrix material properties by transforming growth factor-beta and Runx2 in bone is required for hearing. EMBO Rep. 11 :765–771. [PubMed: 20847738]

Coues, E. Key to North American Birds. 3d. Estes and Lauriat; Boston: 1887.

Dawson MM, Metzger KA, Baier DB, Brainerd EL. 2011; Kinematics of the quadrate bone during feeding in mallard ducks. J Exp Biol. 214 :2036–2046. [PubMed: 21613520]

del Rio A, Perez-Jimenez R, Liu RC, Roca-Cusachs P, Fernandez JM, Sheetz MP. 2009; Stretching single talin rod molecules activates vinculin binding. Science. 323 :638–641. [PubMed: 19179532]

Derynck, R, Piek, E, Schneider, RA, Choy, L, Alliston, T. TGF-β family signalling in mesenchymal differentiation. In: Derynck, R, Miyazono, K, editors. The TGF-beta Family. Cold Spring Harbor Laboratory Press; Cold Spring Harbor, N.Y.: 2008. 613–666.

Dupont S, Morsut L, Aragona M, Enzo E, Giulitti S, Cordenonsi M, Zanconato F, Le Digabel J, Forcato M, Bicciato S, Elvassore N, Piccolo S. 2011; Role of YAP/TAZ in mechanotransduction. Nature. 474 :179–U212. [PubMed: 21654799]

Ealba EL, Jheon AH, Hall J, Curantz C, Butcher KD, Schneider RA. 2015; Neural crest-mediated bone resorption is a determinant of species-specific jaw length. Dev Biol. 408 :151–163. [PubMed: 26449912]

Ealba EL, Schneider RA. 2013; A simple PCR-based strategy for estimating species-specific contributions in chimeras and xenografts. Development. 140 :3062–3068. [PubMed: 23785056]

Eames BF, Schneider RA. 2008; The genesis of cartilage size and shape during development and evolution. Development. 135 :3947–3958. [PubMed: 18987028]

Eames BF, Schneider RA. 2005; Quail-duck chimeras reveal spatiotemporal plasticity in molecular and histogenic programs of cranial feather development. Development. 132 :1499–1509. [PubMed: 15728671]

Edom-Vovard F, Bonnin M, Duprez D. 2001; Fgf8 transcripts are located in tendons during embryonic chick limb development. Mech Dev. 108 :203–206. [PubMed: 11578876]

Edom-Vovard F, Schuler B, Bonnin MA, Teillet MA, Duprez D. 2002; Fgf4 positively regulates scleraxis and tenascin expression in chick limb tendons. Dev Biol. 247 :351–366. [PubMed: 12086472]

Eichele G, Tickle C, Alberts BM. 1984; Microcontrolled release of biologically active compounds in chick embryos: beads of 200-microns diameter for the local release of retinoids. Anal Biochem. 142 :542–555. [PubMed: 6543292]

Eloy-Trinquet S, Wang H, Edom-Vovard F, Duprez D. 2009; Fgf signaling components are associated with muscles and tendons during limb development. Dev Dyn. 238 :1195–1206. [PubMed: 19384958]

Evans DJ, Noden DM. 2006; Spatial relations between avian craniofacial neural crest and paraxial mesoderm cells. Dev Dyn. 235 :1310–1325. [PubMed: 16395689]

Fang J, Hall BK. 1997; Chondrogenic cell differentiation from membrane bone periostea. Anat Embryol. 196 :349–362.

Ferguson CM, Miclau T, Hu D, Alpern E, Helms JA. 1998; Common molecular pathways in skeletal morphogenesis and repair. Ann N Y Acad Sci. 857 :33–42. [PubMed: 9917830]

Fish JL, Schneider RA. 2014a Assessing species-specific contributions to craniofacial development using quail-duck chimeras. J Vis Exp.

Fish, JL, Schneider, RA. Chapter 6 – neural crest-mediated tissue interactions during craniofacial development: the origins of species-specific pattern. In: Trainor, PA, editor. Neural Crest Cells. Academic Press; Boston: 2014b. 101–124.

Fish JL, Sklar RS, Woronowicz KC, Schneider RA. 2014; Multiple developmental mechanisms regulate species-specific jaw size. Development. 141 :674–684. [PubMed: 24449843]

Fitzgerald, TC. The Coturnix Quail; Anatomy and Histology. 1st. Iowa State University Press; Ames: 1969.

Govindarajan V, Overbeek PA. 2006; FGF9 can induce endochondral ossification in cranial mesenchyme. BMC Dev Biol. 6 :7. [PubMed: 16504022]

Grenier J, Teillet MA, Grifone R, Kelly RG, Duprez D. 2009; Relationship between neural crest cells and cranial mesoderm during head muscle development. PLoS One. 4 :e4381. [PubMed: 19198652]

Hall BK. 1967; The formation of adventitious cartilage by membrane bones under the influence of mechanical stimulation applied in vitro. Life Sci. 6 :663–667. [PubMed: 6034183]

Hall BK. 1968; In vitro studies on mechanical evocation of adventitious cartilage in chick. J Exp Zool. 168 :283. [PubMed: 5692733]

Hall BK. 1972; Immobilization and cartilage transformation into bone in embryonic chick. Anat Rec. 173 :391. [PubMed: 4262207]

Hall BK. 1979; Selective proliferation and accumulation of chondroprogenitor cells as the mode of action of biomechanical factors during secondary chondrogenesis. Teratology. 20 :81–91. [PubMed: 515966]

Hall BK. 1986; The role of movement and tissue interactions in the development and growth of bone and secondary cartilage in the clavicle of the embryonic chick. J Embryol Exp Morphol. 93 :133–152. [PubMed: 3734681]

Hall, BK. Bones and Cartilage: Developmental and Evolutionary Skeletal Biology. Elsevier Academic Press; San Diego, Calif: 2005.

Hall BK, Herring SW. 1990; Paralysis and growth of the musculoskeletal system in the embryonic chick. J Morphol. 206 :45–56. [PubMed: 2246789]

Hall J, Jheon AH, Ealba EL, Eames BF, Butcher KD, Mak SS, Ladher R, Alliston T, Schneider RA. 2014; Evolution of a developmental mechanism: species-specific regulation of the cell cycle and the timing of events during craniofacial osteogenesis. Dev Biol. 385 :380–395. [PubMed: 24262986]

Hamburger V, Balaban M, Oppenheim R, Wenger E. 1965; Periodic motility of normal and spinal chick embryos between 8 and 17 days of incubation. J Exp Zool. 159 :1–13. [PubMed: 5215365]

Hamburger V, Hamilton HL. 1951; A series of normal stages in the development of the chick embryo. J Morphol. 88 :49–92. [PubMed: 24539719]

Hamill OP, McBride DW. 1996; The pharmacology of mechanogated membrane ion channels. Pharmacol Rev. 48 :231–252. [PubMed: 8804105]

Hamilton, HL. Lillie's Development of the Chick: An Introduction to Embryology. Third. Holt, Rinehart and Winston; New York: 1965.

Havis E, Bonnin MA, Esteves de Lima J, Charvet B, Milet C, Duprez D. 2016; TGFbeta and FGF promote tendon progenitor fate and act downstream of muscle contraction to regulate tendon differentiation during chick limb development. Development. 143 :3839–3851. [PubMed: 27624906]

Havis E, Bonnin MA, Olivera-Martinez I, Nazaret N, Ruggiu M, Weibel J, Durand C, Guerquin MJ, Bonod-Bidaud C, Ruggiero F, Schweitzer R, Duprez D. 2014; Transcriptomic analysis of mouse limb tendon cells during development. Development. 141 :3683–3696. [PubMed: 25249460]

Hayamizu TF, Sessions SK, Wanek N, Bryant SV. 1991; Effects of localized application of transforming growth factor beta 1 on developing chick limbs. Dev Biol. 145 :164–173. [PubMed: 2019321]

Horowitz SL, Shapiro HH. 1951; Modifications of mandibular architecture following removal of temporalis muscle in the rat. J Dent Res. 30 :276–280. [PubMed: 14824358]

Huang AH, Riordan TJ, Pryce B, Weibel JL, Watson SS, Long F, Lefebvre V, Harfe BD, Stadler HS, Akiyama H, Tufa SF, Keene DR, Schweitzer R. 2015; Musculoskeletal integration at the wrist underlies the modular development of limb tendons. Development. 142 :2431–2441. [PubMed: 26062940]

Huang B, Takahashi K, Sakata-Goto T, Kiso H, Togo Y, Saito K, Tsukamoto H, Sugai M, Akira S, Shimizu A, Bessho K. 2013; Phenotypes of CCAAT/enhancer-binding protein beta deficiency: hyperdontia and elongated coronoid process. Oral Dis. 19 :144–150. [PubMed: 22849712]

Inman GJ, Nicolas FJ, Callahan JF, Harling JD, Gaster LM, Reith AD, Laping NJ, Hill CS. 2002; SB-431542 is a potent and specific inhibitor of transforming growth factor-beta superfamily type I activin receptor-like kinase (ALK) receptors ALK4, ALK5, and ALK7. Mol Pharmacol. 62 :65–74. [PubMed: 12065756]

Jollie MT. 1957; The head skeleton of the chicken and remarks on the anatomy of this region in other birds. J Morphol. 100 :389–436.

Kantomaa, T, Rönning, O. Growth mechanisms of the mandible. In: Dixon, AD, Hoyte, DAN, Rönning, O, editors. Fundamentals of Craniofacial Growth. CRC Press; Boca Raton: 1997. 189–204.

Kardon G. 1998; Muscle and tendon morphogenesis in the avian hind limb. Development. 125 :4019–4032. [PubMed: 9735363]

Kardon G, Harfe BD, Tabin CJ. 2003; A Tcf4-positive mesodermal population provides a prepattern for vertebrate limb muscle patterning. Dev Cell. 5 :937–944. [PubMed: 14667415]

Kawarada Y, Inoue Y, Kawasaki F, Fukuura K, Sato K, Tanaka T, Itoh Y, Hayashi H. 2016; TGF-beta induces p53/Smads complex formation in the PAI-1 promoter to activate transcription. Sci Rep. 6

Kleinnulend J, Roelofsen J, Sterck JGH, Semeins CM, Burger EH. 1995; Mechanical loading stimulates the release of transforming growth-factor-beta activity by cultured mouse calvariae and periosteal cells. J Cell Physiol. 163 :115–119. [PubMed: 7896887]

Koo BS, Song Y, Lee S, Sung YK, Sung IH, Jun JB. 2017 Prevalence and distribution of sesamoid bones and accessory ossicles of the foot as determined by digital tomosynthesis. Clin Anat.

Koecke H. 1958; Normalstadien der Embryonalentwicklung bei der Hausente (Anas boschas domestica). Embryologica. 4 :55–78.

Landmesser L, Morris DG. 1975; The development of functional innervation in the hind limb of the chick embryo. J Physiol. 249 :301–326. [PubMed: 1177095]

Leary, S, Underwood, W, Anthony, R, Cartner, S, Corey, D, Grandin, T, Greenacre, C, Gwaltney-Brant, S, McCrackin, MA, Meye, R, Miller, D, Shearer, J, Yanong, R, Golab, GC, Patterson-Kane, E. AVMA Guidelines for the Euthanasia of Animals. 2013. American Veterinary Medical Association; Schaumburg, IL: 2013.

Le Douarin, NM, Dieterlen-Lievre, F, Teillet, M. Quail-Chick Transplantations. In: Bronner-Fraser, M, editor. Methods in Avian Embryology. Academic Press; San Diego: 1996. 23–59.

Livak KJ, Schmittgen TD. 2001; Analysis of relative gene expression data using real-time quantitative PCR and the 2(-delta delta C(T)) method. Methods. 25 :402–408. [PubMed: 11846609]

Lorda-Diez CI, Montero JA, Martinez-Cue C, Garcia-Porrero JA, Hurle JM. 2009; Transforming growth factors beta coordinate cartilage and tendon differentiation in the developing limb mesenchyme. J Biol Chem. 284 :29988–29996. [PubMed: 19717568]

Lucas, AM, Stettenheim, PR. Avian Anatomy: Integument. United States Department of Agriculture; Washington, D.C.: 1972.

Lwigale PY, Schneider RA. 2008; Other chimeras: quail-duck and mouse-chick. Methods Cell Biol. 87 :59–74. [PubMed: 18485291]

Maeda T, Sakabe T, Sunaga A, Sakai K, Rivera AL, Keene DR, Sasaki T, Stavnezer E, Iannotti J, Schweitzer R, Ilic D, Baskaran H, Sakai T. 2011; Conversion of mechanical force into TGF-beta-mediated biochemical signals. Curr Biol. 21 :933–941. [PubMed: 21600772]

Mammoto T, Ingber DE. 2010; Mechanical control of tissue and organ development. Development. 137 :1407–1420. [PubMed: 20388652]

Mathew SJ, Hansen JM, Merrell AJ, Murphy MM, Lawson JA, Hutcheson DA, Hansen MS, Angus-Hill M, Kardon G. 2011; Connective tissue fibroblasts and Tcf4 regulate myogenesis. Development. 138 :371–384. [PubMed: 21177349]

Matthews BD, Overby DR, Mannix R, Ingber DE. 2006; Cellular adaptation to mechanical stress: role of integrins, Rho, cytoskeletal tension and mechanosensitive ion channels. J Cell Sci. 119 :508–518. [PubMed: 16443749]

McBeath R, Pirone DM, Nelson CM, Bhadriraju K, Chen CS. 2004; Cell shape, cytoskeletal tension, and RhoA regulate stem cell lineage commitment. Dev Cell. 6 :483–495. [PubMed: 15068789]

McLeod, WM. Avian Anatomy. Burgess Pub. Co.; Minneapolis: 1964.

Merrill AE, Eames BF, Weston SJ, Heath T, Schneider RA. 2008; Mesenchyme-dependent BMP signaling directs the timing of mandibular osteogenesis. Development. 135 :1223–1234. [PubMed: 18287200]

Mitgutsch C, Wimmer C, Sanchez-Villagra MR, Hahnloser R, Schneider RA. 2011; Timing of ossification in duck, quail, and zebra finch: intraspecific variation, heterochronies, and life history evolution. Zool Sci. 28 :491–500.

Moore WJ. 1973; An experimental study of the functional components of growth in the rat mandible. Acta Anat. 85 :378–385. [PubMed: 4723385]

Moore, WJ. The Mammalian Skull. Cambridge University Press; Cambridge: 1981.

Moss ML, Meehan MA. 1970; Functional cranial analysis of the coronoid process in the rat. Acta Anat. 77 :11–24. [PubMed: 5504200]

Murakami S, Kan M, McKeehan WL, de Crombrugghe B. 2000; Up-regulation of the chondrogenic Sox9 gene by fibroblast growth factors is mediated by the mitogen-activated protein kinase pathway. Proc Natl Acad Sci USA. 97 :1113–1118. [PubMed: 10655493]

Murchison ND, Price BA, Conner DA, Keene DR, Olson EN, Tabin CJ, Schweitzer R. 2007; Regulation of tendon differentiation by scleraxis distinguishes force-transmitting tendons from muscle-anchoring tendons. Development. 134 :2697–2708. [PubMed: 17567668]

Naderi J, Bernreuther C, Grabinski N, Putman CT, Henkel B, Bell G, Glatzel M, Sultan KR. 2009; Plasminogen activator inhibitor type 1 up-regulation is associated with skeletal muscle atrophy and associated fibrosis. Am J Pathol. 175 :763–771. [PubMed: 19574431]

Nakane Y, Tsudzuki M. 1999; Development of the skeleton in Japanese quail embryos. Dev Growth Differ. 41 :523–534. [PubMed: 10545025]

Nguyen J, Tang SY, Nguyen D, Alliston T. 2013; Load regulates bone formation and sclerostin expression through a TGF beta-dependent mechanism. PLoS One. 8

Niswander L, Tickle C, Vogel A, Booth I, Martin GR. 1993; FGF-4 replaces the apical ectodermal ridge and directs outgrowth and patterning of the limb. Cell. 75 :579–587. [PubMed: 8221896]

Noden, D, Schneider, RA. Neural crest cells and the community of plan for craniofacial development: historical debates and current perspectives. In: Saint-Jeannet, J-P, editor. Neural Crest Induction and Differentiation. Landes Bioscience; Georgetown, Tex: 2006. 1–23.

Noden DM. 1983; The role of the neural crest in patterning of avian cranial skeletal, connective, and muscle tissues. Dev Biol. 96 :144–165. [PubMed: 6825950]

Noden DM. 1988; Interactions and fates of avian craniofacial mesenchyme. Development. 103 :121–140. [PubMed: 3074905]

Noden DM, Trainor PA. 2005; Relations and interactions between cranial mesoderm and neural crest populations. J Anat. 207 :575–601. [PubMed: 16313393]

Oka K, Oka S, Hosokawa R, Bringas P, Brockhoff HC, Nonaka K, Chai Y. 2008; TGF-beta mediated Dlx5 signaling plays a crucial role in osteochondroprogenitor cell lineage determination during mandible development. Dev Biol. 321 :303–309. [PubMed: 18684439]

Oka K, Oka S, Sasaki T, Ito Y, Bringas P, Nonaka K, Chai Y. 2007; The role of TGF-beta signaling in regulating chondrogenesis and osteogenesis during mandibular development. Dev Biol. 303 :391–404. [PubMed: 17204263]

Ornitz DM, Marie PJ. 2015; Fibroblast growth factor signaling in skeletal development and disease. Genes Dev. 29 :1463–1486. [PubMed: 26220993]

Padgett CS, Ivey WD. 1960; The normal embryology of the Coturnix quail. Anat Rec. 137 :1–11. [PubMed: 14429703]

Pitsillides AA. 2006; Early effects of embryonic movement: ‘a shot out of the dark’. J Anat. 208 :417–431. [PubMed: 16637868]

Pollard AS, McGonnell IM, Pitsillides AA. 2014; Mechanoadaptation of developing limbs: shaking a leg. J Anat. 224 :615–623. [PubMed: 24635640]

Presnell, JK, Schreibman, MP. Humason’s Animal Tissue Techniques. Johns Hopkins University Press; Baltimore, USA: 1997.

Pruitt BL, Dunn AR, Weis WI, Nelson WJ. 2014; Mechano-transduction: from molecules to tissues. PLoS Biol. 12

Pryce BA, Watson SS, Murchison ND, Staverosky JA, Duker N, Schweitzer R. 2009; Recruitment and maintenance of tendon progenitors by TGF beta signaling are essential for tendon formation. Development. 136 :1351–1361. [PubMed: 19304887]

Quinn TP, Schlueter M, Soifer SJ, Gutierrez JA. 2002; Cyclic mechanical stretch induces VEGF and FGF-2 expression in pulmonary vascular smooth muscle cells. Am J Physiol Lung Cell Mol Physiol. 282 :L897–L903. [PubMed: 11943652]

Raizman I, De Croos JN, Pilliar R, Kandel RA. 2010; Calcium regulates cyclic compression-induced early changes in chondrocytes during in vitro cartilage tissue formation. Cell Calcium. 48 :232–242. [PubMed: 20932575]

Ramage L, Nuki G, Salter DM. 2009; Signalling cascades in mechanotransduction: cell-matrix interactions and mechanical loading. Scand J Med Sci Sports. 19 :457–469. [PubMed: 19538538]

Rinon A, Lazar S, Marshall H, Buchmann-Moller S, Neufeld A, Elhanany-Tamir H, Taketo MM, Sommer L, Krumlauf R, Tzahor E. 2007; Cranial neural crest cells regulate head muscle patterning and differentiation during vertebrate embryogenesis. Development. 134 :3065–3075. [PubMed: 17652354]

Ricklefs, RE, Starck, JM. Embryonic Growth and Development. In: Starck, JM, Ricklefs, RE, editors. Avian growth and development : evolution within the altricial-precocial spectrum. Oxford University Press; New York: 1998. 31–58.

Robbins JR, Evanko SP, Vogel KG. 1997; Mechanical loading and TGF-beta regulate proteoglycan synthesis in tendon. Arch Biochem Biophys. 342 :203–211. [PubMed: 9186480]

Roberts SR, Knight MM, Lee DA, Bader DL. 2001; Mechanical compression influences intracellular Ca(2+) signaling in chondrocytes seeded in agarose constructs. J Appl Physiol. 90 :1385–1391. [PubMed: 11247938]

Robling AG, Kang KS, Bullock WA, Foster WH, Murugesh D, Loots GG, Genetos DC. 2016; Sost, independent of the non-coding enhancer ECR5, is required for bone mechanoadaptation. Bone. 92 :180–188. [PubMed: 27601226]

Robling AG, Niziolek PJ, Baldridge LA, Condon KW, Allen MR, Alam I, Mantila SM, Gluhak-Heinrich J, Bellido TM, Harris SE, Turner CH. 2008; Mechanical stimulation of bone in vivo reduces osteocyte expression of Sost/sclerostin. J Biol Chem. 283 :5866–5875. [PubMed: 18089564]

Rolfe RA, Nowlan NC, Kenny EM, Cormican P, Morris DW, Prendergast PJ, Kelly D, Murphy P. 2014; Identification of mechanosensitive genes during skeletal development: alteration of genes associated with cytoskeletal rearrangement and cell signalling pathways. BMC Genom. 15 :48.

Rot-Nikcevic I, Downing KJ, Hall BK, Kablar B. 2007; Development of the mouse mandibles and clavicles in the absence of skeletal myogenesis. Histol Histopathol. 22 :51–60. [PubMed: 17128411]

Russell, ES. Form and Function: A Contribution to the History of Animal Morphology. John Murray Publishers Ltd; London: 1916.

Sanford LP, Ormsby I, GittenbergerdeGroot AC, Sariola H, Friedman R, Boivin GP, Cardell EL, Doetschman T. 1997; TGF beta 2 knockout mice have multiple developmental defects that are nonoverlapping with other TGF beta knockout phenotypes. Development. 124 :2659–2670. [PubMed: 9217007]

Schneider RA. 1999; Neural crest can form cartilages normally derived from mesoderm during development of the avian head skeleton. Dev Biol. 208 :441–455. [PubMed: 10191057]

Schneider RA. 2005; Developmental mechanisms facilitating the evolution of bills and quills. J Anat. 207 :563–573. [PubMed: 16313392]

Schneider RA. 2007; How to tweak a beak: molecular techniques for studying the evolution of size and shape in Darwin's finches and other birds. Bioessays. 29 :1–6. [PubMed: 17187350]

Schneider RA. 2015; Regulation of jaw length during development, disease, and evolution. Curr Top Dev Biol. 115 :271–298. [PubMed: 26589929]

Schneider, RA. Cellular Control of Time, Size, and Shape in Development and Evolution. In: Hall, BK, Moody, S, editors. Cells in Evolutionary Biology: Translating Genotypes into Phenotypes – Past, Present, Future. CRC Press, Taylor & Francis Group; Boca Raton: 2018a. 167–212.

Schneider RA. 2018b Neural crest and the origins of species-specific pattern. Genesis.

Schneider RA, Helms JA. 2003; The cellular and molecular origins of beak morphology. Science. 299 :565–568. [PubMed: 12543976]

Schneider RA, Hu D, Rubenstein JL, Maden M, Helms JA. 2001; Local retinoid signaling coordinates forebrain and facial morphogenesis by maintaining FGF8 and SHH. Development. 128 :2755–2767. [PubMed: 11526081]

Schweitzer R, Chyung JH, Murtaugh LC, Brent AE, Rosen V, Olson EN, Lassar A, Tabin CJ. 2001; Analysis of the tendon cell fate using Scleraxis, a specific marker for tendons and ligaments. Development. 128 :3855–3866. [PubMed: 11585810]

Schweitzer R, Zelzer E, Volk T. 2010; Connecting muscles to tendons: tendons and musculoskeletal development in flies and vertebrates (vol. 137, pg 2807, 2010). Development. 137 :Ee47–Ee47.

Shakibaei M, Mobasheri A. 2003; Beta1-integrins co-localize with Na, K-ATPase, epithelial sodium channels (ENaC) and voltage activated calcium channels (VACC) in mechanoreceptor complexes of mouse limb-bud chondrocytes. Histol Histopathol. 18 :343–351. [PubMed: 12647783]

Sharir A, Stern T, Rot C, Shahar R, Zelzer E. 2011; Muscle force regulates bone shaping for optimal load-bearing capacity during embryogenesis. Development. 138 :3247–3259. [PubMed: 21750035]

Shi M, Zhu J, Wang R, Chen X, Mi L, Walz T, Springer TA. 2011; Latent TGF-beta structure and activation. Nature. 474 :343–349. [PubMed: 21677751]

Shibata S, Suda N, Fukada K, Ohyama K, Yamashita Y, Hammond VE. 2003; Mandibular coronoid process in parathyroid hormone-related protein-deficient mice shows ectopic cartilage formation accompanied by abnormal bone modeling. Anat Embryol. 207 :35–44.

Shufeldt, RW. Osteology of Birds University of the State of New York. Albany: 1909.

Shwartz Y, Blitz E, Zelzer E. 2013; One load to rule them all: mechanical control of the musculoskeletal system in development and aging. Differentiation. 86 :104–111. [PubMed: 23953954]

Shwartz Y, Farkas Z, Stern T, Aszodi A, Zelzer E. 2012; Muscle contraction controls skeletal morphogenesis through regulation of chondrocyte convergent extension. Dev Biol. 370 :154–163. [PubMed: 22884393]

Smith TG, Sweetman D, Patterson M, Keyse SM, Munsterberg A. 2005; Feedback interactions between MKP3 and ERK MAP kinase control scleraxis expression and the specification of rib progenitors in the developing chick somite. Development. 132 :1305–1314. [PubMed: 15716340]

Smith FJ, Percival CJ, Young NM, Hu D, Schneider RA, Marcucio RS, Hallgrimsson B. 2015 Divergence of craniofacial developmental trajectories among avian embryos. Dev Dyn.

Solem RC, Eames BF, Tokita M, Schneider RA. 2011; Mesenchymal and mechanical mechanisms of secondary cartilage induction. Dev Biol. 356 :28–39. [PubMed: 21600197]

Soni NN, Malloy RB. 1974; Effect of removal of the temporal muscle on the coronoid process in guinea pigs: quantitative triple fluorochrome study. J Dent Res. 53 :474–480. [PubMed: 4521911]

Starck, JM, Ricklefs, RE. Avian growth and development : evolution within the altricial-precocial spectrum. Oxford University Press; New York: 1998.

Starck JM. 1989; Zeitmuster der Ontogenesen bei nestflüchtenden und nesthockenden Vögeln. Cour Forsch-Inst Senckenberg. 114 :1–319.

Stutzmann J, Petrovic A. 1975; Nature and evolutive aptitudes of cells of the mitotic compartment of the secondary cartilages of the mandible and maxilla of the young rat. Experience with cytotypic culture and homotransplantation. Bull l'Assoc Anat. 59 :523–534.

Subramanian A, Schilling TF. 2015; Tendon development and musculoskeletal assembly: emerging roles for the extracellular matrix. Development. 142 :4191–4204. [PubMed: 26672092]

Sugimoto Y, Takimoto A, Akiyama H, Kist R, Scherer G, Nakamura T, Hiraki Y, Shukunami C. 2013; Scx+/Sox9+ progenitors contribute to the establishment of the junction between cartilage and tendon/ligament. Development. 140 :2280–2288. [PubMed: 23615282]

Sun L, Tran N, Liang C, Tang F, Rice A, Schreck R, Waltz K, Shawver LK, McMahon G, Tang C. 1999; Design, synthesis, and evaluations of substituted 3-[(3- or 4-carboxyethylpyrrol-2-yl)methylidenyl]indolin-2-ones as inhibitors of VEGF, FGF, and PDGF receptor tyrosine kinases. J Med Chem. 42 :5120–5130. [PubMed: 10602697]

Sun L, Tran N, Tang F, App H, Hirth P, McMahon G, Tang C. 1998; Synthesis and biological evaluations of 3-substituted indolin-2-ones: a novel class of tyrosine kinase inhibitors that exhibit selectivity toward particular receptor tyrosine kinases. J Med Chem. 41 :2588–2603. [PubMed: 9651163]

Tanck E, Blankevoort L, Haaijman A, Burger EH, Huiskes R. 2000; Influence of muscular activity on local mineralization patterns in metatarsals of the embryonic mouse. J Orthop Res. 18 :613–619. [PubMed: 11052498]

Thompson DW. 1942 On Growth and Form.

Tokita M, Schneider RA. 2009; Developmental origins of species-specific muscle pattern. Dev Biol. 331 :311–325. [PubMed: 19450573]

Tu XL, Rhee Y, Condon KW, Bivi N, Allen MR, Dwyer D, Stolina M, Turner CH, Robling AG, Plotkin LI, Bellido T. 2012; Sost downregulation and local Wnt signaling are required for the osteogenic response to mechanical loading. Bone. 50 :209–217. [PubMed: 22075208]

Tucker AS, Lumsden A. 2004; Neural crest cells provide species-specific patterning information in the developing branchial skeleton. Evol Dev. 6 :32–40. [PubMed: 15108816]

Van den Heuvel WF. 1992; Kinetics of the skull in the chicken (Gallus Gallus domesticus). Neth J Zool. 42 :561–582.

Vincent T, Hermansson M, Bolton M, Wait R, Saklatvala J. 2002; Basic FGF mediates an immediate response of articular cartilage to mechanical injury. Proc Natl Acad Sci USA. 99 :8259–8264. [PubMed: 12034879]

Vincent TL, McLean CJ, Full LE, Peston D, Saklatvala J. 2007; FGF-2 is bound to perlecan in the pericellular matrix of articular cartilage, where it acts as a chondrocyte mechanotransducer. Osteoarthr Cartil. 15 :752–763.

Vinkka H. 1982; Secondary cartilages in the facial skeleton of the rat. Proc Finn Dent Soc Suom Hammaslaak Toim. 78 (Suppl. 7) :S1–S137.

Wang N, Tytell JD, Ingber DE. 2009; Mechanotransduction at a distance: mechanically coupling the extracellular matrix with the nucleus. Nat Rev Mol Cell Biol. 10 :75–82. [PubMed: 19197334]

Washburn SL. 1947; The relation of the temporal muscle to the form of the skull. Anat Rec. 99 :239–248. [PubMed: 20270605]

Wassersug RJ. 1976; A procedure for differential staining of cartilage and bone in whole formalin-fixed vertebrates. Stain Technol. 51 :131–134. [PubMed: 59420]

Wen J, Tao H, Lau K, Liu H, Simmons CA, Sun Y, Hopyan S. 2017; Cell and tissue scale forces coregulate Fgfr2-dependent tetrads and rosettes in the mouse embryo. Biophys J. 112 :2209–2218. [PubMed: 28538157]

Wipff PJ, Rifkin DB, Meister JJ, Hinz B. 2007; Myofibroblast contraction activates latent TGF-beta1 from the extracellular matrix. J Cell Biol. 179 :1311–1323. [PubMed: 18086923]

Wu KC, Streicher J, Lee ML, Hall BK, Muller GB. 2001; Role of motility in embryonic development I: embryo movements and amnion contractions in the chick and the influence of illumination. J Exp Zool. 291 :186–194. [PubMed: 11479917]

Yamashita T, Sohal GS. 1987; Embryonic origin of skeletal muscle cells in the iris of the duck and quail. Cell Tissue Res. 249 :31–37. [PubMed: 3621295]

Young NM, Hu D, Lainoff AJ, Smith FJ, Diaz R, Tucker AS, Trainor PA, Schneider RA, Hallgrimsson B, Marcucio RS. 2014; Embryonic bauplans and the developmental origins of facial diversity and constraint. Development. 141 :1059–1063. [PubMed: 24550113]

Zacchei AM. 1961; The embryonic development of the Japanese quail (Coturnix coturnix japonica). Arch Ital Anat Embriol. 66 :36–62. [PubMed: 13787591]

Zusi, RL. Patterns of diversity in the avian skull. In: Hanken, J, Hall, BK, editors. The Skull. First. University of Chicago Press; Chicago: 1993. 391–437.

Zweers G. 1974; Structure, movement, and myography of the feeding apparatus of the mallard (Anas platyrhynchos L.). A study in functional anatomy. Neth J Zool. 24 (4) :323–467.

Zweers, GA, Gerritsen, AFC, Kranenburg-Voogd, PJv. Mechanics of Feeding of the Mallard (Anas platyrhynchos L; Aves, Anseriformes): The Lingual Apparatus and the Suction-pressure Pump Mechanism of Straining. S Karger; Basel, New York: 1977a.

Zweers GA, Kunz G, Mos J. 1977b; Functional anatomy of the feeding apparatus of the mallard (Anas platyrhynchos L.) structure, movement, electromyography and electroneurography. Anat Anz. 142 :10–20. [PubMed: 596635]

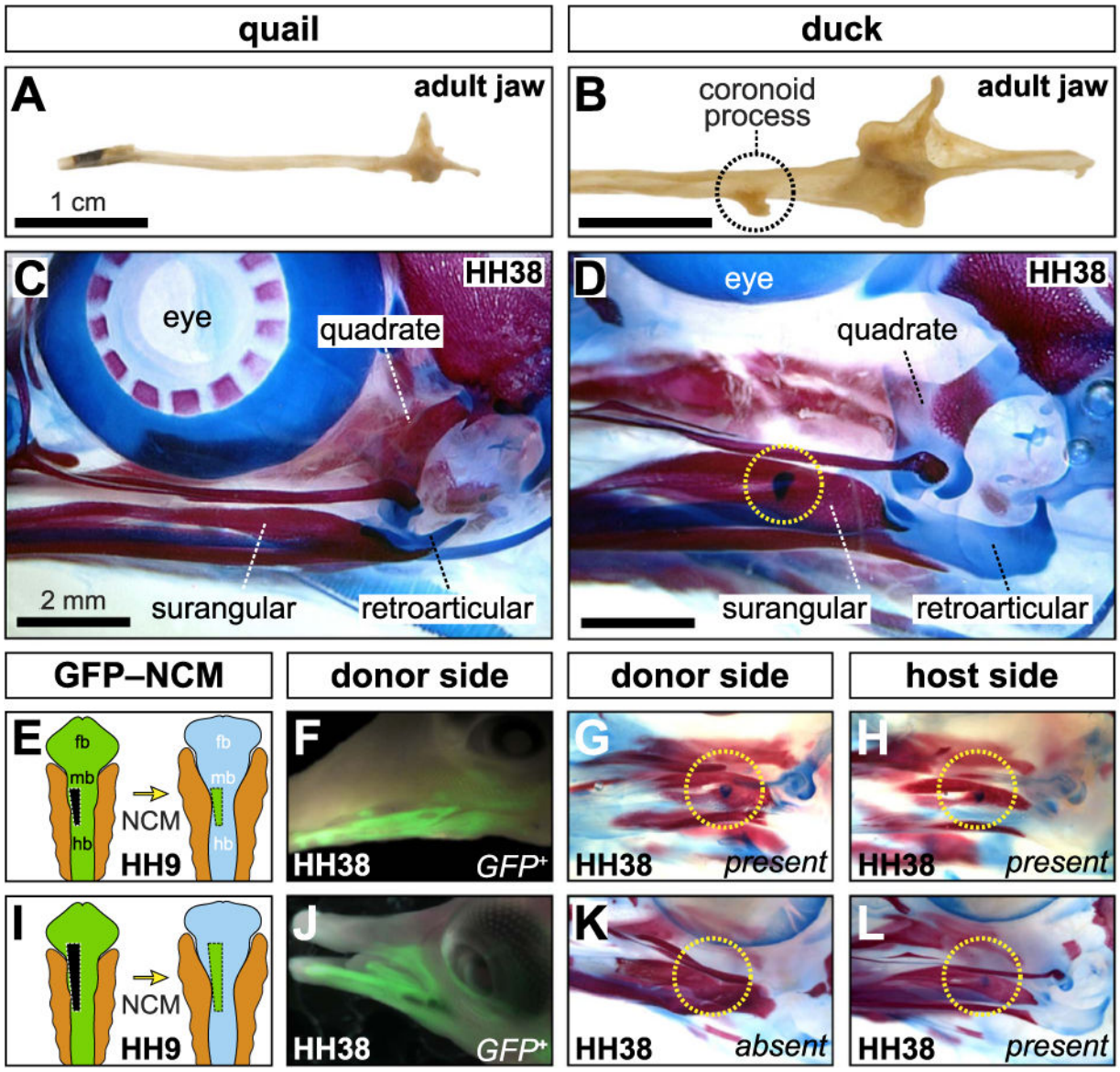

Fig. 1. Species-Specific form of the jaw and role of NCM

(**A, B**) Ventral views of left mandibles reveal the smooth appearance in quail and laterally protruding coronoid process in duck (dashed circle). (**C, D**) Left lateral views of cleared and stained skulls showing cartilage (blue) and bone (red). A secondary cartilage forms on the lateral surface of the surangular in duck but not in quail. (**E**) Chimeric "chuck" were produced by unilaterally transplanting small NCM grafts from the midbrain and hindbrain of a GFP-positive chick donor into a comparable position in a stage-matched duck-host. (**F**) Small GFP-chick transplants yield a limited distribution of NCM-derived connective tissues. (**G, H**) The chick-donor side shows little transformation and resembles the contralateral control duck side with secondary cartilage present. (**I**–**L**) Larger NCM grafts distribute GFP-positive cells more broadly and lead to a loss of secondary cartilage relative to the contralateral, duck-host side.

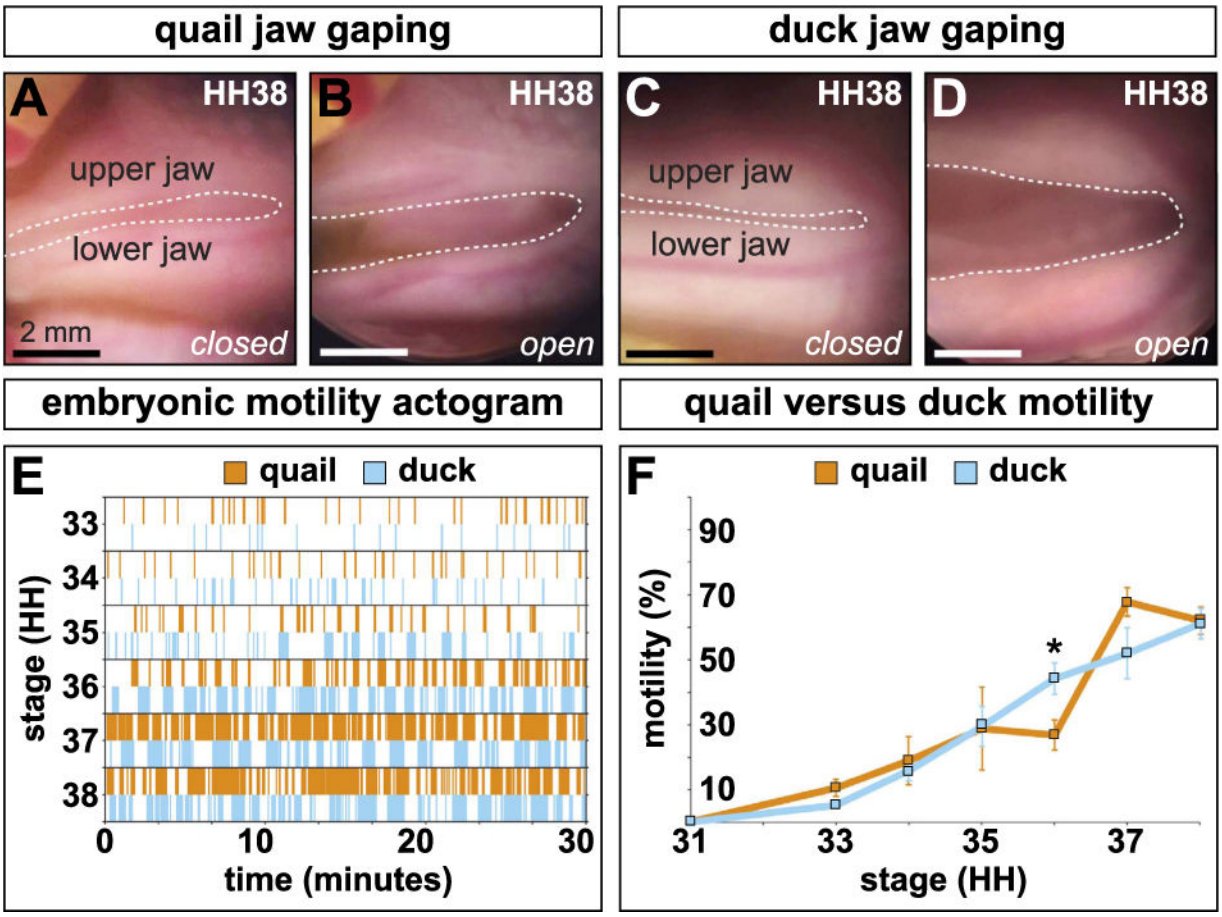

Fig. 2. Jaw motility in ovo

(**A**–**D**) Representative open and closed jaw gaping positions in quail and duck embryos. (**E**) Actogram of 30-min observation periods for representative quail and duck. Six consecutive stages were observed. Quail and duck activity periods steadily increase in frequency and duration. (**F**) During HH33, a key stage of secondary cartilage induction, the differences in jaw motility are minimal with quail being slightly more active, though the difference is not significant. Duck are significantly more active at HH36 ($p < 0.0005$).

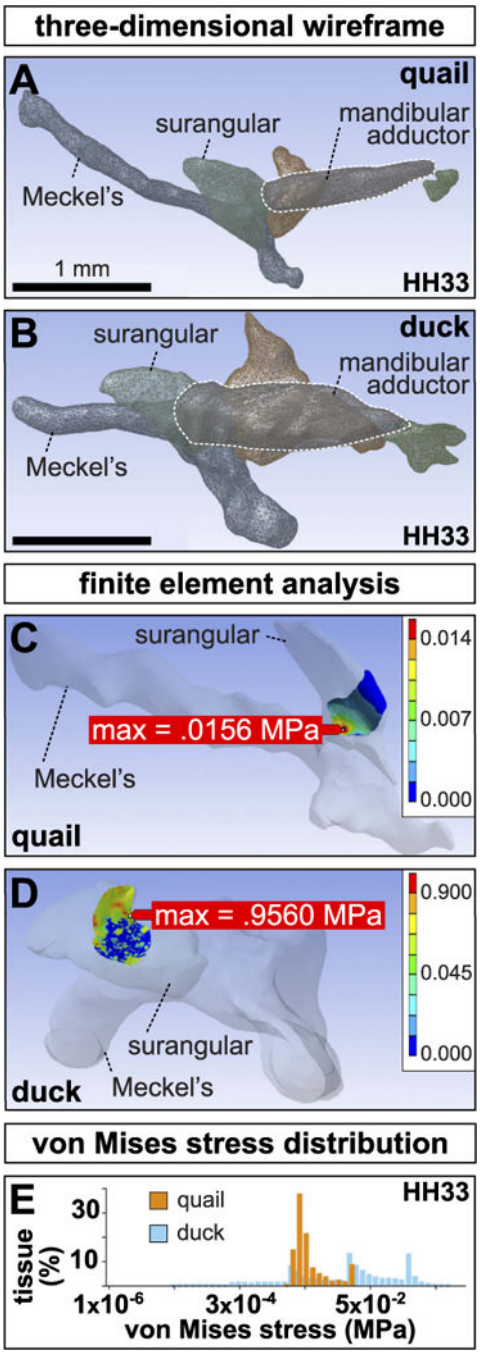

Fig. 3. 3D reconstructions and finite element analysis of the adductor complex

Three-dimensional wireframes of left (**A**) quail and (**B**) duck jaw showing the presumptive surangular (light-green), quadrate (red), mandibular adductor muscle (purple, outlined in white), post-orbital (dark-green), and Meckel's (blue). Note the slender mandibular adductor and its dorsal insertion on the quail surangular versus the bulky mandibular adductor and its lateral insertion in duck. (**C**) Finite element modeling predicts a maximum von Mises stress concentration of 0.0156 MPa within the medial portion of the contact area between the mandibular adductor and the surangular in quail. Color scales indicate predicted von Mises

stress. (**D**) A maximum von Mises stress concentration of 0.9560 MPa is predicted within a dorsolateral region in duck. (**E**) Histogram of the range of von Mises stresses in duck versus quail. Note that the maximum von Mises stress in quail is substantially less than in duck.

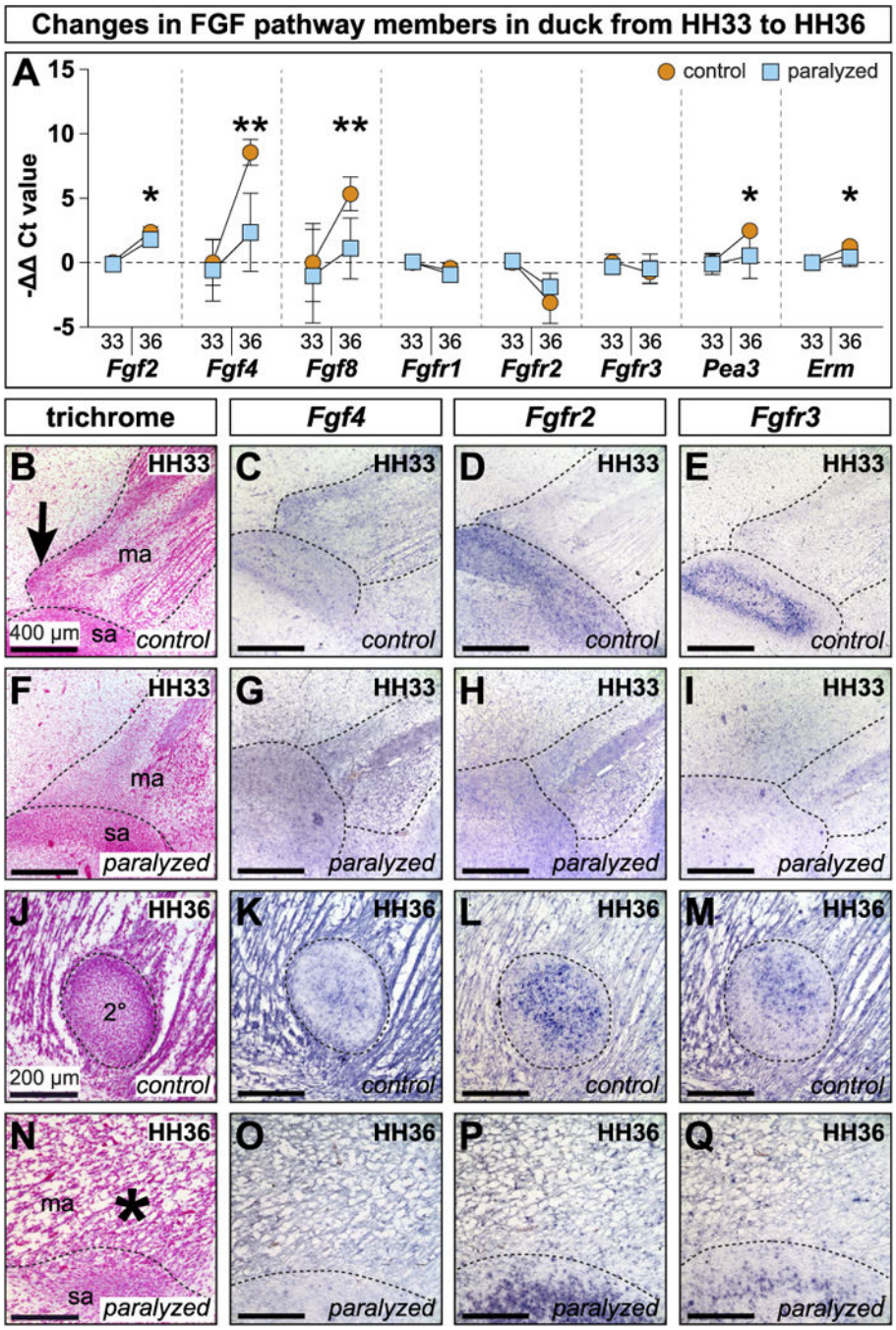

Fig. 4. FGF pathway in paralyzed and control duck

(**A**) Differential expression in isolated mandibular adductor entheses from HH33 and HH36 control and paralyzed embryos. Each gene is normalized to *β-Actin* and shown relative to HH33 controls. Error bars represent standard deviation. Asterisks denote statistical significance between control and paralyzed samples at HH36 (*$p < 0.05$; **$p < 0.005$). (**B**) Sagittal section through the mandibular adductor (ma) muscle insertion along the presumptive surangular (sa) bone. A secondary cartilage condensation is present at the mandibular adductor insertion on the coronoid process (arrow). (**C, D**) *Fgf4* and *Fgfr2*

(stained purple) are expressed in the secondary cartilage condensation and surrounding tissues. (**E**) *Fgfr3* is expressed around the margins of the surangular condensation. (**F**) 24 h after paralysis at HH32, HH33 embryos show disrupted muscle and tendon, and there is no secondary cartilage condensation. (**G,H**) *Fgf4* and *Fgfr2* are altered and the secondary cartilage is absent. (**I**) *Fgfr3* is disrupted. (**J**) Sagittal section through the mandibular adductor muscle insertion on the coronoid process lateral to the surangular. The secondary cartilage (2°) is well formed. (**K**–**M**) *Fgf4*, *Fgfr2*, and *Fgfr3* are in the secondary cartilage and surrounding tissues. (**N**) Paralysis at HH32 prevents secondary cartilage formation (asterisk). The mandibular adductor inserts directly onto the surangular. (**O**–**Q**) *Fgf4, Fgfr2, and Fgfr3* are altered and secondary cartilage is absent.

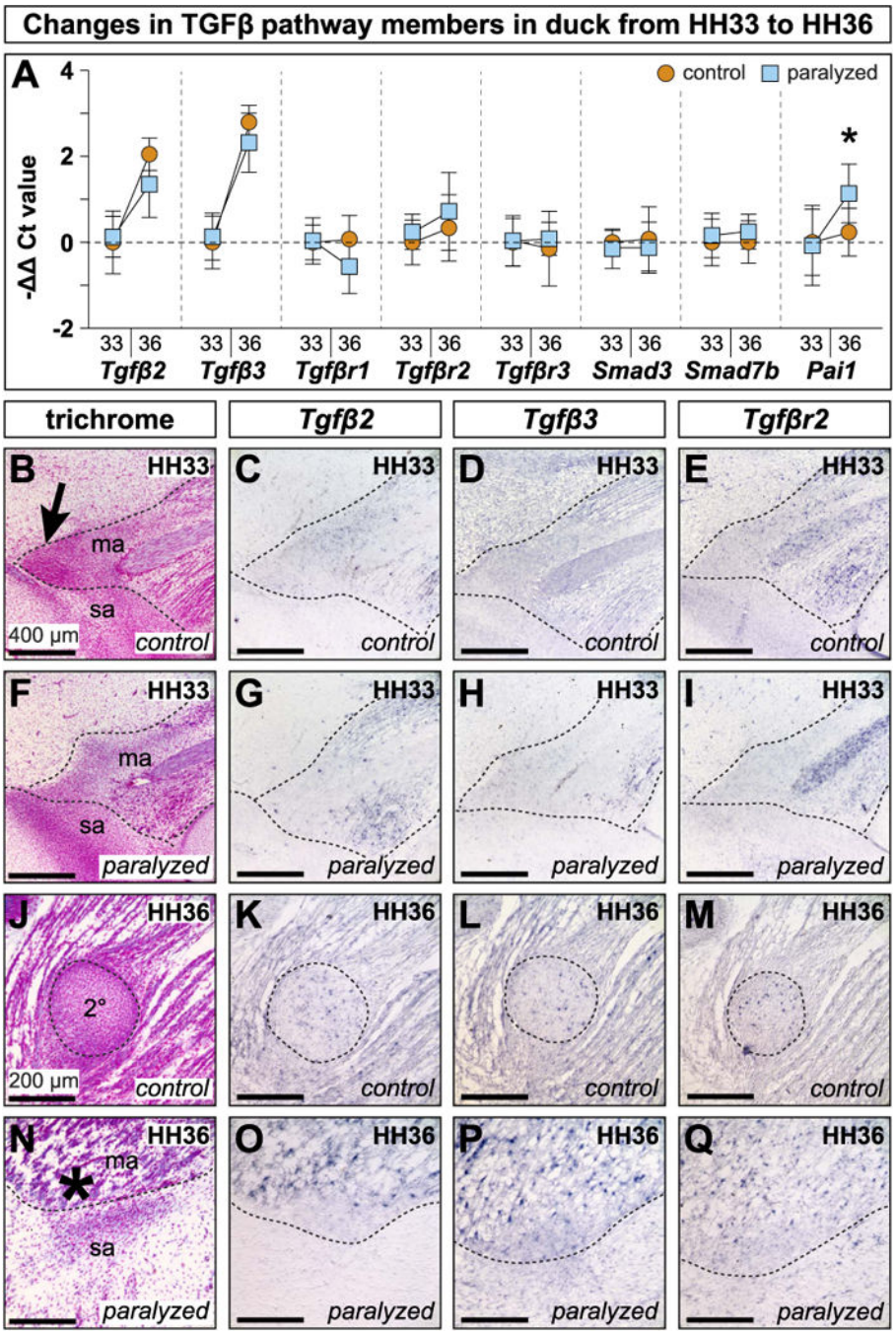

Fig. 5. TGFβ pathway in paralyzed and control duck

(**A**) Differential expression in isolated mandibular adductor entheses from HH33 and HH36 control and paralyzed embryos. Each gene is normalized to *β-Actin* and displayed relative to HH33 controls. Error bars represent standard deviation. Asterisk denote statistical significance between control and paralyzed samples at HH36 (*p < 0.05). (**B**) Sagittal section through the mandibular adductor (ma) muscle insertion along the presumptive surangular (sa) bone. A secondary cartilage condensation is present at the mandibular adductor insertion on the coronoid process (arrow). (**C**–**E**) *Tgfβ2*, *Tgfβ3*, and *Tgfβr2* are

expressed in the secondary cartilage condensation and surrounding tissues. (**F**) 24 h after paralysis at HH32, HH33 embryos show disrupted muscle and tendon, and there is no secondary cartilage condensation. (**G–I**) *Tgfβ2*, *Tgfβ3*, and *Tgfβr2* are disrupted. There is no secondary cartilage condensation. (**J**) Sagittal section through the mandibular adductor muscle insertion on the coronoid process lateral to the surangular. The secondary cartilage (2°) is well formed. (**K–M**) *Tgfβ2*, *Tgfβ3*, and *Tgfβr2* are expressed in the secondary cartilage and surrounding tissues. (**N**) Paralysis at HH32 prevents secondary cartilage formation (asterisk). (**O–Q**) *Tgfβ2*, *Tgfβ3*, and *Tgfβr2* are altered and secondary cartilage is absent.

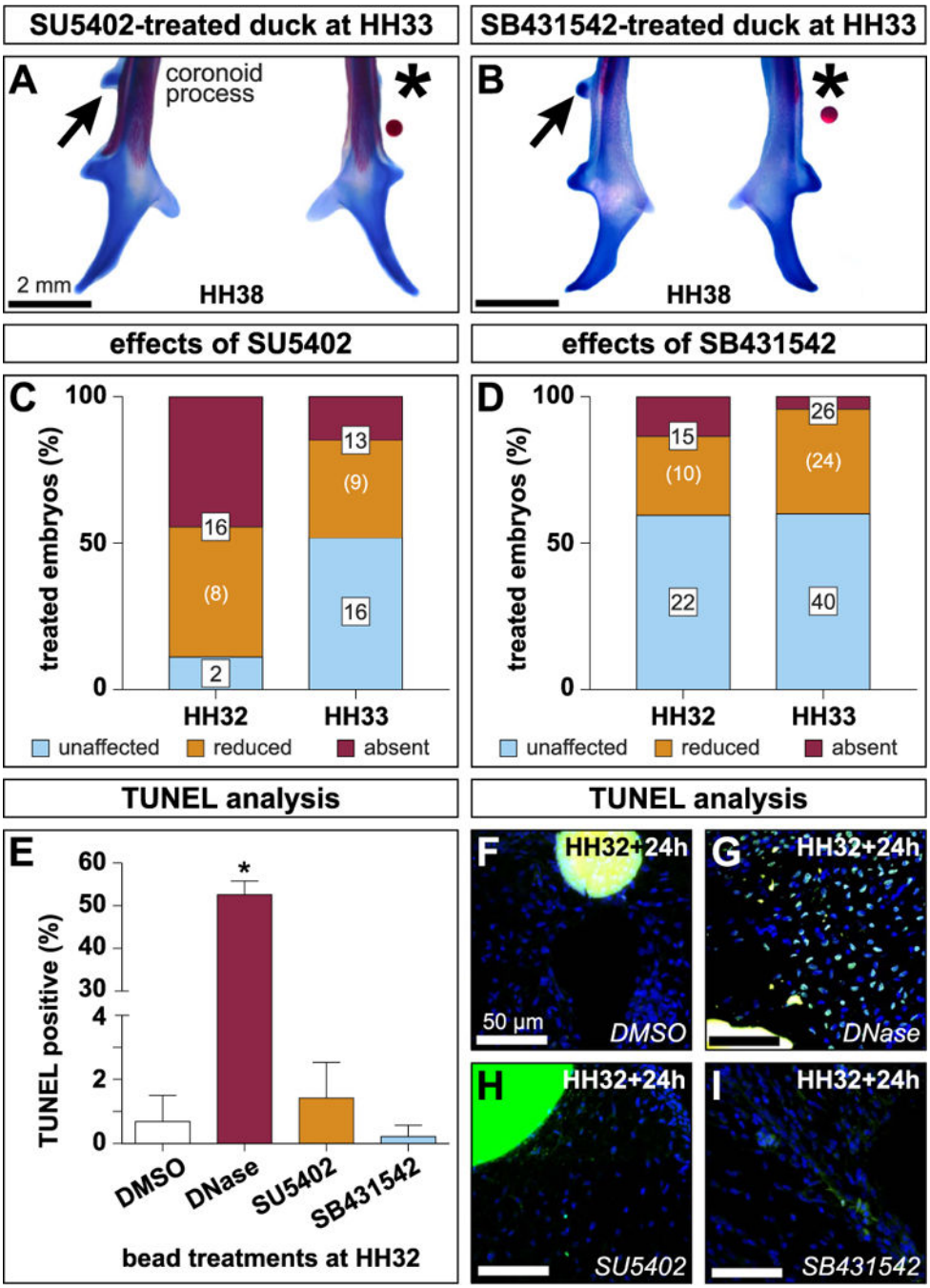

Fig. 6. Inhibition of FGF and TGFβ signaling during secondary chondrogenesis

(**A**) Ventral view of a cleared and stained duck mandible treated with a bead soaked in an FGF inhibitor (SU5402). Note the loss of secondary cartilage (asterisk) while the untreated side develops normally (arrow). (**B**) Inhibition of TGFβ signaling (SB431542) results in a loss of secondary cartilage while the control side develops normally. (**C**) FGF signaling inhibition eliminates or reduces secondary cartilage by HH38, with a greater treatment effect at HH32 versus HH33 (Fisher's Exact Test $p < 0.005$). (**D**) TGFβ signaling inhibition eliminates or reduces secondary cartilage by HH38. (**E**) Inhibiting FGF or TGFβ signaling

does not increase apoptosis after 24 h. Positive control, DNase digested slides displayed significant apoptosis (unpaired *t*-test $p < 0.0001$). (**F**–**I**) Sections from DMSO, SU5402, or SB431542 treated embryos reveal little apoptosis. Extensive positive staining was observed in DNase digested sections.

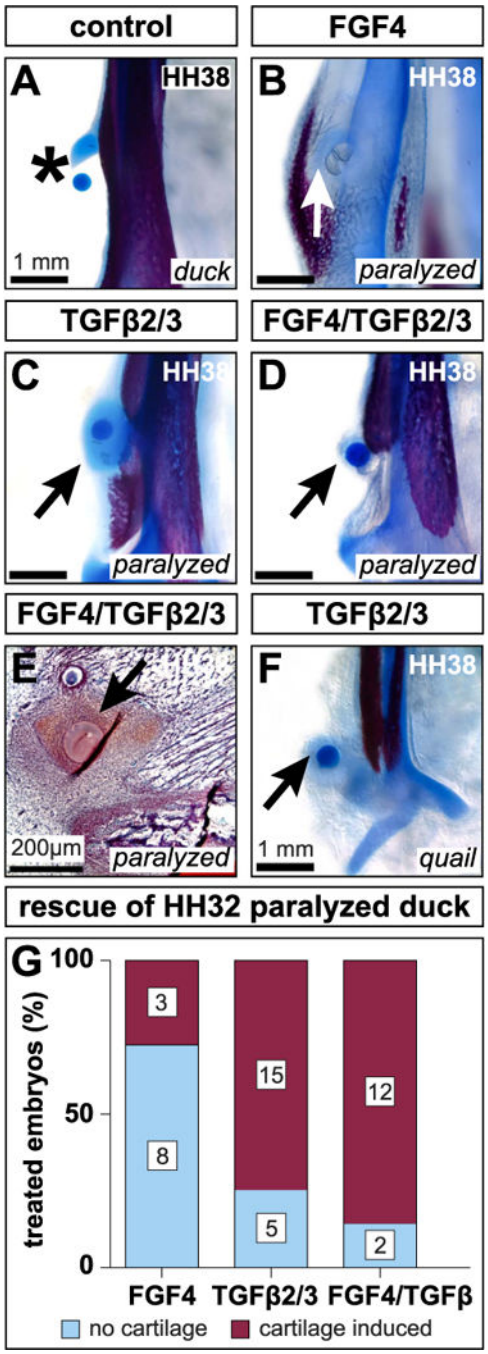

Fig. 7. FGF4 and TGFβ2/TGF0β3 induce chondrogenesis

(**A**) Ventral view of a cleared and stained mandible treated with a BSA soaked bead. Carrier treatments exert no effect on secondary cartilage (asterisk). (**B**) HH32 FGF4 treatment induces cartilage (arrow) in paralyzed embryos by HH38. (**C**) TGFβ2/TGFβ3 treatment induces cartilage (arrow) in paralyzed embryos. (**D**) Combined FGF4 and TGFβ2/TGFβ3 treatments induce cartilage (arrow) despite paralysis. (**E**) HH38 sagittal section through the mandibular adductor insertion of a paralyzed embryo implanted with FGF4 and TGFβ2/TGFβ3 beads at HH32. Safranin-O reveals dense, positively stained mesenchyme

surrounding the beads (arrow). (**F**) HH32 TGFβ2/TGFβ3 treatment induces quail to form cartilage by HH38 (arrow). (**G**) FGF4, TGFβ2/TGFβ3, and FGF4/TGFβ2/TGFβ3 treatments induce cartilage by HH38. The distribution of treatment outcomes depends upon the ligand or ligands embryos receive (Fisher's Exact Test $p = 0.005$).

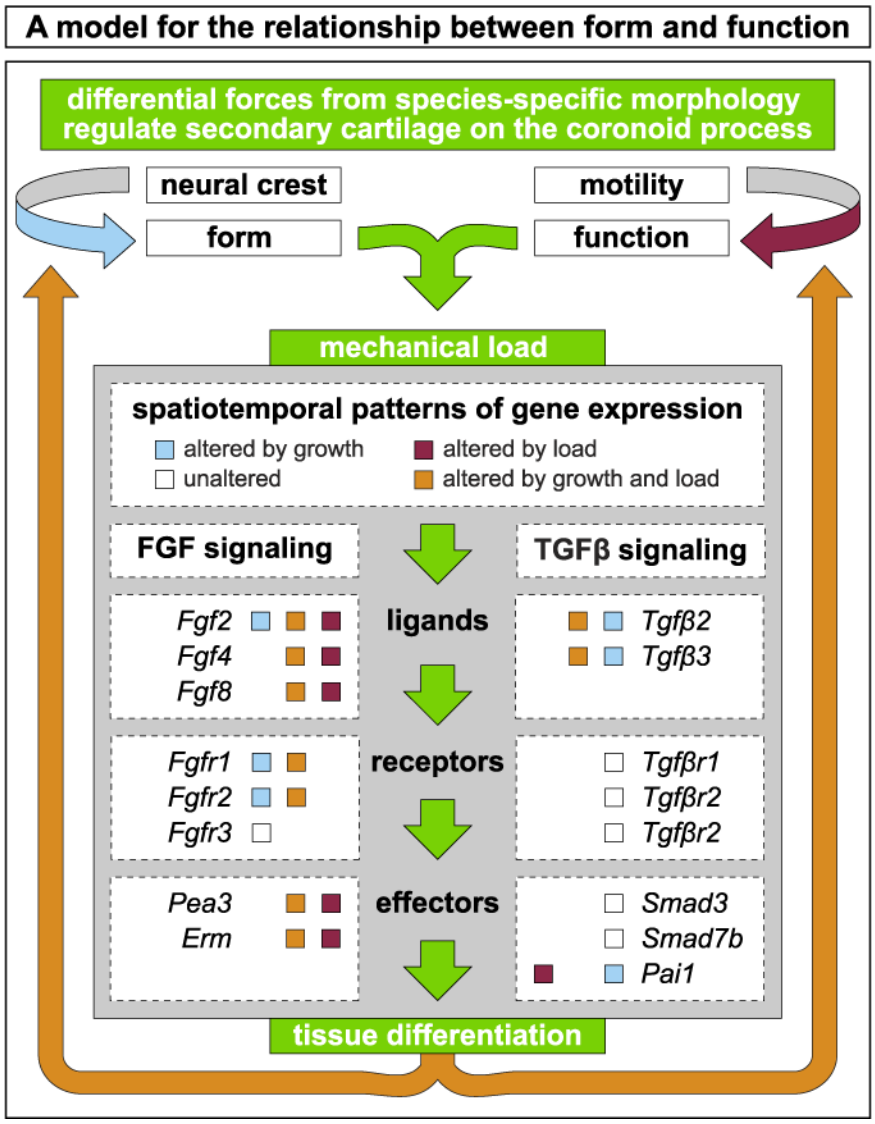

Fig. 8. A model integrating form and function with FGF and TGFβ signaling

NCM-mediated species-specific jaw geometry, (i.e., dorsal versus lateral mandibular adductor insertions) and functional loading by embryonic motility contribute to differential forces and tissue differentiation. The resultant mechanical stress leads to differential activation of FGF and TGFβ signaling and regulates the presence or absence of secondary cartilage on the coronoid process. We observe three overlapping patterns of expression: One set is altered by growth (blue boxes), another altered by load (red boxes), and a third is altered by both growth and load (orange boxes). A fourth set of genes remains unaltered both during growth and despite a loss of embryonic motility (white boxes). Some genes are found in multiple sets, reflecting the complex integration of form and function during embryonic development.

Table 1

Spatial localization of gene expression in HH33 and HH36 control duck.

			FGF signaling pathway					TGFβ signaling pathway			
Structure	**Tissue type**		**Fgf4**	**Fgf8**	**Fgfr2**	**Fgfr3**	**Pea3**	**Tgfβ2**	**Tgfβ3**	**Tgfβr2**	**Smad3**
Control Duck at HH33											
Meckel's Cartilage	Primary Cartilage	Perichondrium[1]			X		X				
		Cartilage[2]	X	X	X	X	X		X	X	X
Coronoid Process	Secondary Cartilage	Condensation	X	X	X		X	X	X	X	X
Surangular	Bone	Condensation[3]	X	X	X	X	X				
Mandibular Adductor	Muscle[4]		X	X			X	X	X	X	X
Muscle Insertion	Tendon		X	X			X	X	X	X	X

			FGF signaling pathway					TGFβ signaling pathway			
Structure	Tissue type		*Fgf4*	*Fgf8*	*Fgfr2*	*Fgfr3*	*Pea3*	*Tgfβ2*	*Tgfβ3*	*Tgfβr2*	*Smad3*
Control Duck at HH36											
Meckel's Cartilage	Primary Cartilage	Perichondrium	X		X	X	X	X	X		X
		Cartilage	X	X	X	X	X	X	X		X
Coronoid Process	Secondary Cartilage	Perichondrium		X				X	X		X
		Cartilage[5]	X	X	X	X	X	X	X	X	X
Surangular	Bone	Periosteum[6]	X	X	X	X	X	X	X		X
		Bone	X	X	X	X	X	X	X	X	X
Mandibular Adductor	Muscle[7]		X	X	X	X	X	X	X		X
Muscle Insertion	Tendon		X	X	X	X	X	X	X		X

[1] Strong *Fgfr2* expression throughout the perichondrium with isolated cells expressing *Pea3.*

[2] Strong *Fgfr3* expression throughout with isolated cells expressing *Fgf8* and *Pea3.*

[3] Strong *Fgfr2* expression throughout the surangular condensation with isolated *Pea3* expressing cells.

[4] *Fgf4* and *Pea3* expression appear strongest near muscle tips while *Tgfβ2* is strongly expressed throughout the muscle.

[5] Strong *Fgfr2* expression throughout while *Fgfr3* expression is spatially restricted to the center.

Dev Biol. Author manuscript; available in PMC 2019 December 01.

[6] *Fgfr2* and *Fgfr3* are expressed throughout bone, but periosteal expression is quite strong.

[7] *Smad3* expression strongest near muscle insertions.